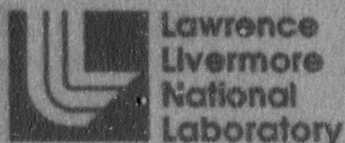

SCANS (Shipping Cask ANalysis System)
A Microcomputer Based Analysis System
for Shipping Cask Design Review

Volume 4--Theory Manual
Thermal Analysis

G. L. Johnson and A. B. Shapiro

Prepared for
U.S. Nuclear Regulatory Commission



B904110465 B90228
PDR NUREG
CR-4554 R PDR

AVAILABILITY NOTICE

Availability of Reference Materials Cited in NRC Publications

Most documents cited in NRC publications will be available from one of the following sources:

1. The NRC Public Document Room, 2120 L Street, NW, Lower Level, Washington, DC 20555
2. The Superintendent of Documents, U.S. Government Printing Office, P.O. Box 37082, Washington, DC 20413-7082
3. The National Technical Information Service, Springfield, VA 22161

Although the listing that follows represents the majority of documents cited in NRC publications, it is not intended to be exhaustive.

Referenced documents available for inspection and copying for a fee from the NRC Public Document Room include NRC correspondence and internal NRC memoranda; NRC Office of Inspection and Enforcement bulletins, circulars, information notices, inspection and investigation notices; Licensee Event Reports; vendor reports and correspondence; Commission papers; and applicant and licensee documents and correspondence.

The following documents in the NUREG series are available for purchase from the GPO Sales Program: formal NRC staff and contractor reports, NRC-sponsored conference proceedings, and NRC booklets and brochures. Also available are Regulatory Guides, NRC regulations in the *Code of Federal Regulations*, and *Nuclear Regulatory Commission Issuances*.

Documents available from the National Technical Information Service include NUREG series reports and technical reports prepared by other federal agencies and reports prepared by the Atomic Energy Commission, forerunner agency to the Nuclear Regulatory Commission.

Documents available from public and special technical libraries include all open literature items, such as books, journal and periodical articles, and transactions. *Federal Register* notices, federal and state legislation, and congressional reports can usually be obtained from these libraries.

Documents such as theses, dissertations, foreign reports and translations, and non-NRC conference proceedings are available for purchase from the organization sponsoring the publication cited.

Single copies of NRC draft reports are available free, to the extent of supply, upon written request to the Office of Information Resources Management, Distribution Section, U.S. Nuclear Regulatory Commission, Washington, DC 20555.

Copies of industry codes and standards used in a substantive manner in the NRC regulatory process are maintained at the NRC Library, 7920 Norfolk Avenue, Bethesda, Maryland, and are available there for reference use by the public. Codes and standards are usually copyrighted and may be purchased from the originating organization or, if they are American National Standards, from the American National Standards Institute, 1430 Brinleyway, New York, NY 10018.

DISCLAIMER NOTICE

This report was prepared as an account of work sponsored by an agency of the United States Government. Neither the United States Government nor any agency thereof, or any of their employees, makes any warranty, expressed or implied, or assumes any legal liability of responsibility for any third party's use, or the results of such use, of any information, apparatus, product or process disclosed in this report, or represents that its use by such third party would not infringe privately owned rights.

SCANS (Shipping Cask ANalysis System)
A Microcomputer Based Analysis System
for Shipping Cask Design Review

Volume 4--Theory Manual
Thermal Analysis

G. L. Johnson and A. B. Shapiro

Prepared for
U.S. Nuclear Regulatory Commission



8904110465 890228
PDR NUREG
CR-4554 R PDR

AVAILABILITY NOTICE

Availability of Reference Materials Cited in NRC Publications

Most documents cited in NRC publications will be available from one of the following sources:

1. The NRC Public Document Room, 2120 L Street, NW, Lower Level, Washington, DC 20555
2. The Superintendent of Documents, U.S. Government Printing Office, P.O. Box 37082, Washington, DC 20013-7082
3. The National Technical Information Service, Springfield, VA 22161

Although the listing that follows represents the majority of documents cited in NRC publications, it is not intended to be exhaustive.

Referenced documents available for inspection and copying for a fee from the NRC Public Document Room include NRC correspondence and internal NRC memoranda; NRC Office of Inspection and Enforcement bulletins, circulars, information notices, inspection and investigation notices; Licensee Event Reports; vendor reports and correspondence; Commission papers; and applicant and licensee documents and correspondence.

The following documents in the NUREG series are available for purchase from the GPO Sales Program: formal NRC staff and contractor reports, NRC-sponsored conference proceedings, and NRC booklets and brochures. Also available are Regulatory Guides, NRC regulations in the *Code of Federal Regulations*, and *Nuclear Regulatory Commission Issuances*.

Documents available from the National Technical Information Service include NUREG series reports and technical reports prepared by other federal agencies and reports prepared by the Atomic Energy Commission, forerunner agency to the Nuclear Regulatory Commission.

Documents available from public and special technical libraries include all open literature items, such as books, journal and periodical articles, and transactions. *Federal Register* notices, federal and state legislation, and congressional reports can usually be obtained from these libraries.

Documents such as theses, dissertations, foreign reports and translations, and non-NRC conference proceedings are available for purchase from the organization sponsoring the publication cited.

Single copies of NRC draft reports are available free, to the extent of supply, upon written request to the Office of Information Resources Management, Distribution Section, U.S. Nuclear Regulatory Commission, Washington, DC 20555.

Copies of industry codes and standards used in a substantive manner in the NRC regulatory process are maintained at the NRC Library, 7920 Norfolk Avenue, Bethesda, Maryland, and are available there for reference use by the public. Codes and standards are usually copyrighted and may be purchased from the originating organization or, if they are American National Standards, from the American National Standards Institute, 1430 Broadway, New York, NY 10018.

DISCLAIMER NOTICE

This report was prepared as an account of work sponsored by an agency of the United States Government. Neither the United States Government nor any agency thereof, or any of their employees, makes any warranty, expressed or implied, or assumes any legal liability of responsibility for any third party's use, or the results of such use, of any information, apparatus, product or process disclosed in this report, or represents that its use by such third party would not infringe privately owned rights.

SCANS (Shipping Cask ANalysis System)
A Microcomputer Based Analysis System
for Shipping Cask Design Review

Volume 4--Theory Manual
Thermal Analysis

Manuscript Completed: January 1989
Date Published: February 1989

Prepared by
G. L. Johnson and A. B. Shapiro

Lawrence Livermore National Laboratory
7000 East Avenue
Livermore, CA 94550

Prepared for
Division of Engineering
Office of Nuclear Regulatory Research
U.S. Nuclear Regulatory Commission
Washington, DC 20555
NRC FIN A0374

ABSTRACT

TOPAZ is the two-dimensional, implicit, finite-element computer code included in the SCANS cask analysis system for heat conduction calculations. TOPAZ, a code developed on LLNL mainframes, has been implemented on IBM PC computers. This report provides documentation of TOPAZ controls and variables and a description of the numerical algorithms used. Sample problems with analytical solutions are presented.

TABLE OF CONTENTS

	<u>Page</u>
Abstract	iii
List of Figures	vii
List of Tables	ix
Nomenclature	xi
Acknowledgments	xiii
Executive Summary	xv
1.0 Introduction	1
2.0 General Theory	2
2.1 Conduction of Heat in an Orthotropic Solid	2
2.2 Finite Element Formulation	3
2.3 Time Integration Scheme	8
2.4 Thermal Contact Resistance Across an Interface (Slidelines)	10
2.5 Enclosure Radiation	14
3.0 Aspects of Topaz	20
3.1 Bandwidth Minimization	20
3.2 Boundary Conditions	20
3.3 Bulk Fluid	23
3.4 Element Types	24
3.5 Energy Balances	24
3.6 Function Definitions	24
3.7 Heat Generation	25
3.8 Initial Conditions	25
3.9 Internal Boundary Elements	26
3.10 Material Properties	26
3.11 Mesh Generation	27
3.12 Nonlinear Analysis	27
3.13 Phase Change	28
3.14 Post Processing	28
3.15 Radiation in Enclosures	28

TABLE OF CONTENTS (con't)

3.16	Slidelines - Thermal Contact Resistance Across an Interface	29
3.17	Steady-State Analysis	30
3.18	Thermal Stress Analysis	30
3.19	Transient Analysis	30
3.20	Units.....	30
4.0	Examples	31
4.1	Introduction.....	31
4.2	Example 1 - Finite Cylinder with 2 Surface Temperatures	31
4.3	Example 2 - Slab with Nonlinear Material Properties	34
4.4	Example 3 - Cylinder with Temperature + Convection Boundary Conditions	37
4.5	Example 4 - One-Dimensional Cylinder with Heat-Generating Core	39
4.6	Example 5 - Finite Rod with Band Heating.....	42
4.7	Example 6 - Finite Cylinder with Strip Heating and Cooling	44
4.8	Example 7 - Finite Hollow Cylinder with Inside Band Heating.....	46
4.9	Example 8 - Regulation Case-Normal Hot Day with Maximum Decay Heat/Solar Heat	48
4.10	Example 9 - Regulation Case-Cold Soak with Maximum Decay Heat/No Solar Heat.....	52
5.0	References.....	54

LIST OF FIGURES

		Page
Figure 2-1	Two-dimensional heat conduction with heat flow at external boundary	2
Figure 2-2	Solid body overlayed with a quadrilateral grid.....	6
Figure 2-3	Bilinear quadrilateral element domain.....	6
Figure 2-4	Added elements for contact resistance or slideline.....	11
Figure 2-5	Typical triangular element at gap or slideline.....	11
Figure 2-6	Relationship between local and global coordinates.....	14
Figure 2-7	Boundary conductions at wall surface	15
Figure 3-1	Direction of outward normal vector with respect to nodes	20
Figure 3-2	Setting boundary linearly varying flux boundary conditions on surface segment.....	21
Figure 3-3	Heat flow between bulk node (B) and adjoining surface (S).....	23
Figure 3-4	Degeneration from four node into three node element	24
Figure 3-5	Piecewise linear curve for interpolation.....	25
Figure 3-6	Thermal coupling between two surfaces.....	26
Figure 3-7	Orthotropic material angle (ψ)	27
Figure 3-8	Relationship of boundaries for an enclosure	28
Figure 3-9	Relationship between slave and master surfaces.....	29
Figure 4-1	Solid finite cylinder with two surface temperatures	31
Figure 4-2	Analytical and numerical results for a steady-state heat flow in a finite cylinder with two surface temperatures	33
Figure 4-3	Heat conduction in homogeneous isotropic slab.....	34
Figure 4-4	Finite solid cylinder with convection.....	37
Figure 4-5	Analytical and numerical results of temperature plus convection boundary conditions in a cylinder	38
Figure 4-6	SNL Model 1 geometry and LLNL finite element mesh.....	39
Figure 4-7	Analytical and numerical results for one dimensional cylinder with internal heating.....	41
Figure 4-8	Finite rod with heating band	42
Figure 4-9	Analytical and numerical results for steady-state heat flow in a finite rod with band heating.....	43
Figure 4-10	Finite cylinder with strip heating and cooling.....	44
Figure 4-11	Analytical and numerical results for steady-state heat flow in a finite cylinder with strip heating and cooling	45

LIST OF FIGURES (con't)

Figure 4-12	Finite hollow cylinder with inside band heating	46
Figure 4-13	Analytical and numerical results for steady-state heat flow in a finite hollow cylinder with inside band heating.....	47
Figure 4-14	Geometry and finite element mesh for regulation case. Normal hot with maximum heat.....	48
Figure 4-15	Comparison between the CRAY version of TOPAZ and the PC version of TOPAZ for Example 8.....	51
Figure 4-16	Comparison between the CRAY version of TOPAZ and the PC version of TOPAZ for Example 9.....	53

LIST OF TABLES

	<u>Page</u>
Table 4-1 Input data for Example 1.....	32
Table 4-2 Input data for Example 2.....	35
Table 4-3 Comparison of results for Example 2.....	36
Table 4-4 Input data for Example 3.....	37
Table 4-5 Input data for Example 4.....	40
Table 4-6 Input data for Example 5.....	42
Table 4-7 Input data for Example 6.....	44
Table 4-8 Input data for Example 7.....	46
Table 4-9 Stainless steel specific heat capacity and thermal conductivity.....	49
Table 4-10 Lead specific heat capacity and thermal conductivity.....	49
Table 4-11 Polyurethane foam specific heat capacity and thermal conductivity.....	50

NOMENCLATURE

[Units: M = mass, L = length, E = energy, θ = temperature, T = time]

ρ	=	density [M/L^3]
c	=	specific heat capacity [$E/M\theta$]
θ, T	=	temperature [θ]
t	=	time [T]
x (or r)	=	coordinate in x direction (or radial direction) [L]
y (or z)	=	coordinate in y direction (or axial direction) [L]
k_x (or k_y)	=	thermal conductivity in x direction (or y direction) [$E/LT\theta$]
n_x (or n_y)	=	fraction of bounding surface unit normal in x direction (or y direction)
q_g	=	volumetric heat generation [E/L^3T]
β	=	coefficient relating environment-imposed surface heat loads to environment temperature [$E/L^2T\theta$]
γ	=	parameter defining environment-imposed surface heat loads which are not driven by the environment temperature [E/L^2T]
q_f	=	environment-imposed surface heat flux [E/L^2T]
\dot{q}	=	local net heat flux [E/L^2T]
ω	=	weighting function for integration
h_c	=	convective heat transfer coefficient [$E/L^2T\theta$]
θ_∞, T_∞	=	temperature of environment
T_{surf}	=	boundary surface temperature [θ]
σ	=	Stefan-Boltzman coefficient for thermal radiation heat transfer [$E/L^2T\theta^4$]
\mathcal{F}	=	exchange factor for thermal radiation
θ_i, T_∞	=	temperature at each node
N_i	=	Finite element shape factor
α	=	fraction of time step at which to evaluate solution matrices (see pages 9 - 11)
ψ	=	angle of slideline surfaces to global coordinates
H_i	=	radiant flux incident on a surface i (irradiance) [E/L^2T]
B_j	=	radiation leaving surface j (radiosity) [E/L^2T]
ϵ_j	=	emissivity of radiating surface j
α_i	=	absorptance of emitting surface i
ρ_i	=	reflectivity of surface $i = (1 - \alpha_i)$
A_i	=	area of surface segment i [L^2]
F_{ij}	=	geometric view factor between surface segments i and j
Pr	=	Prandtl Number = ratio of kinematic viscosity to thermal diffusivity

- Gr_L = Grashof Number = ratio of buoyancy forces to viscous forces in a free convection flow
 k_f = thermal conductivity of flowing medium in environment (evaluated at $T_f = (T_{surf} + T_{\infty}) / 2$ [E/TL θ])
 ν_f = kinematic viscosity of flowing medium in environment (evaluated at $T_f = (T_{surf} + T_{\infty}) / 2$ [L²/T])
 β_f = volume expansion coefficient of environment [1/ θ]
 L = characteristic length of surface exposed to natural convection [L]
 g = acceleration due to gravity [L/T²]

ACKNOWLEDGMENTS

The authors would like to thank H. Graves and W. Campbell, technical monitors at the U.S. Nuclear Regulatory Commission for their support and technical direction in the development of the SCANS thermal and pressure stress modules and documentation. Many thanks to M. Kamelgarn for editing.

EXECUTIVE SUMMARY

Lawrence Livermore National Laboratory has developed a microcomputer-based analysis system to assist the Nuclear Regulatory Commission in performing confirmatory analyses for licensing review of radioactive-material shipping cask designs.

This volume (Volume 4) is the Thermal Analysis Theory Manual. In this manual we describe the thermal analysis computer code TOPAZ which is incorporated into the Shipping Container Analysis System (SCANS). Benchmarking example problems are also presented.

SCANS (Shipping Cask ANalysis System)

Volume 4--Theory Manual

Thermal Analysis*

1.0 INTRODUCTION

TOPAZ is the two-dimensional implicit finite element computer code for heat conduction analysis included in the Shipping Container ANalysis System (SCANS). This report documents the equations solved and gives a description of the numerical algorithms used. Sample problems with analytical solutions are presented. TOPAZ has been implemented on IBM PCs.

SCANS is a system of menus and programs used on PCs to complete thermal and impact analyses of type B shipping cask designs being reviewed for certification by the U.S. Nuclear Regulatory Commission. The thermal loads required by NRC regulations are built into SCANS. SCANS includes an input data editor, a finite element mesh generator, analytic codes to predict thermal and structural response, and codes to graphically display the meshes and the results from the analyzers.

TOPAZ can be used to solve for the steady-state or transient temperature field on two-dimensional planar or axisymmetric geometries. Material properties may be temperature-dependent and either isotropic or orthotropic. A variety of time- and temperature-dependent boundary conditions can be specified; these include temperature, flux, convection, and radiation. TOPAZ can solve problems of diffuse band radiation in an enclosure coupled with conduction in the material surrounding the enclosure. Additional features include analyses of thermal contact resistance across an interface, bulk fluids, phase change, and energy balances.

2.0 GENERAL THEORY

2.1 Conduction of Heat in an Orthotropic Solid

The differential equation of conduction of heat in a two-dimensional solid is given by

$$\rho c \frac{\partial \theta}{\partial t} = \frac{\partial}{\partial x} k_x \frac{\partial \theta}{\partial x} + \frac{\partial}{\partial y} k_y \frac{\partial \theta}{\partial y} + q_g \text{ in the volume } \Omega \quad (1)$$

subject to the boundary condition

$$k_x \frac{\partial \theta}{\partial x} n_x + k_y \frac{\partial \theta}{\partial y} n_y + \beta (\theta - \theta_\infty) = \gamma \text{ on the boundary surfaces } \Gamma \quad (2)$$

and with the initial condition

$$\theta = \theta(x, y) \quad \text{at } t = t_0. \quad (3)$$

Equations (1)-(3) represent the strong form of a boundary value problem to be solved for the temperature field within the solid as shown in Fig. 2-1.

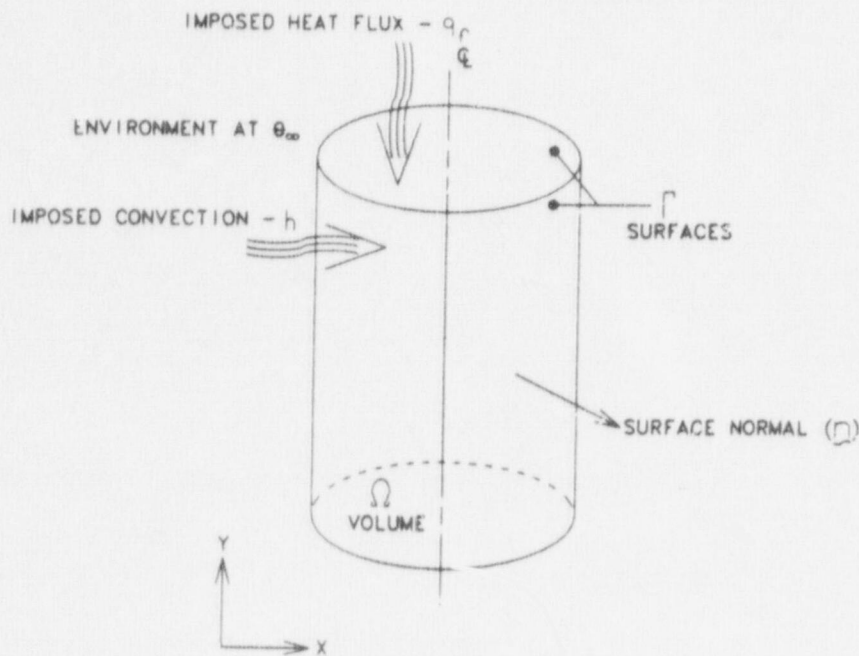


Figure 2-1 Two-dimensional heat conduction with heat flow at external boundary.

2.2 Finite Element Formulation

A weak form of this boundary value problem is obtained by requiring each side of Eq. (1) to be satisfied in an average sense.

$$\iint_{\Omega} \omega \rho c \frac{\partial \theta}{\partial t} dx dy = \iint_{\Omega} \omega \left[\frac{\partial}{\partial x} k_x \frac{\partial \theta}{\partial y} + \frac{\partial}{\partial y} k_y \frac{\partial \theta}{\partial x} \right] dx dy + \iint_{\Omega} \omega q_g dx dy . \quad (4)$$

The weighting function, ω , is any function of x and y that is sufficiently well-behaved that the integrals make sense. Integrating the first term on the right side of Eq. (4) by parts results in a weak form of the boundary value problem (see Appendix 3 of [1]).

$$\begin{aligned} \text{time dependency} & \quad \iint_{\Omega} \omega \rho c \frac{\partial \theta}{\partial t} dx dy = \\ \text{heat conduction} & \quad - \iint_{\Omega} \left[\frac{\partial \omega}{\partial x} k_x \frac{\partial \theta}{\partial x} + \frac{\partial \omega}{\partial y} k_y \frac{\partial \theta}{\partial y} \right] dx dy \\ \text{natural boundary condition} & \quad + \iint_{\Gamma} \omega \left[k_x \frac{\partial \theta}{\partial x} n_x + k_y \frac{\partial \theta}{\partial y} n_y \right] d\Gamma \\ \text{internal heat generation} & \quad + \iint_{\Omega} \omega q_g dx dy . \end{aligned} \quad (5)$$

Notice the appearance of the "natural" boundary condition term in Eq. (5) resulting from the integration by parts operation. Several forms of the boundary condition Eq. (2) will now be substituted for the natural boundary condition term. Equation (2) can be rewritten as

$$k_x \frac{\partial \theta}{\partial x} n_x + k_y \frac{\partial \theta}{\partial y} n_y = \gamma - \beta (\theta - \theta_{\infty}). \quad (6)$$

Heat flow in the TOPAZ computer code is positive in the direction of the surface-outward normal vector. A flux (or Neumann type) boundary condition on a surface segment can be represented by specifying

$$\beta = 0, \quad (\text{FLUX B.C.}) \quad (7)$$

$$\gamma = -q_f.$$

in Eq. (6). A convection (or Robin type) boundary condition can be represented by specifying

$$\beta = h_c, \quad (\text{CONVECTION B.C.}) \quad (8)$$

$$\gamma = 0.$$

in Eq. (6). Equation (8) can also be used for a radiation boundary condition by utilizing a radiant-heat transfer coefficient.

$$h_r = \sigma F (\theta + \theta_{\infty}) (\theta^2 + \theta_{\infty}^2). \quad (\text{RADIATION B.C.}) \quad (9)$$

The forced (or Dirichlet type) boundary condition in which the **TEMPERATURE** is specified on the boundary is imposed on the final system of equations by a penalty method.

For now, let a heat flux be applied on the boundary segment, Γ_f , and heat transfer occur by convection on the boundary segment, Γ_c . Utilizing Eqs. (6) - (8), Eq. (5) becomes

$$\begin{aligned} \text{time dependency} & \quad \iint_{\Omega} \omega \rho c \frac{\partial \theta}{\partial t} dx dy = \\ \text{heat conduction} & \quad - \iint_{\Omega} \left[\frac{\partial \omega}{\partial x} k_x \frac{\partial \theta}{\partial x} + \frac{\partial \omega}{\partial y} k_y \frac{\partial \theta}{\partial y} \right] dx dy \\ \text{flux b.c.} & \quad - \int_{\Gamma_f} \omega q_f d\Gamma_f \\ \text{convection b.c.} & \quad \left\{ \begin{aligned} & + \int_{\Gamma_c} \omega h_c \theta_{\infty} d\Gamma_c \\ & - \int_{\Gamma_c} \omega h_c \theta d\Gamma_c \end{aligned} \right. \\ \text{internal heat generation} & \quad + \iint_{\Omega} \omega q_g dx dy \end{aligned} \quad (10)$$

Galerkin's method consists of seeking an approximate solution to Eq. (10). This proceeds by assuming a trial (shape) function expansion for θ ,

$$\theta = \sum_{i=1}^n N_i \theta_i = N\theta \quad (11a)$$

and taking as the weighting function

$$\omega = N_i \quad (11b)$$

Using the relations Eq. (11) in Eq. (10) results in

$$\begin{aligned} \left[\iint_{\Omega} N_i \rho c N \, dx dy \right] \left\{ \frac{\partial \theta}{\partial t} \right\} &= \left[- \iint_{\Omega} \nabla^T N_i K \nabla N \, dx dy \right] \{ \theta \} \\ - \int_{\Gamma_f} N_i q_f \, d\Gamma_f + \int_{\Gamma_c} N_i h_c \theta_{\infty} \, d\Gamma_c - \left[\int_{\Gamma_c} N_i h_c N \, d\Gamma_c \right] \{ \theta \} & \\ + \iint_{\Omega} N_i q_g \, dx dy & \end{aligned} \quad (12)$$

where

$$(i=1,2,\dots,n)$$

or a set of discrete equations of the form

$$[C] \{\dot{\theta}\} + [H] \{\theta\} = \{F\} \quad (13)$$

with

$$[C_{ij}] = \iint_{\Omega} N_i \rho c N_j \, dx dy \quad (14a)$$

$$[H_{ij}] = \iint_{\Omega} \nabla^T N_i K \nabla N_j \, dx dy + \int_{\Gamma_c} N_i h_c N_j \, d\Gamma_c \quad (14b)$$

$$\{F_i\} = \iint_{\Omega} N_i q_g \, dx dy - \int_{\Gamma_f} N_i q_f \, d\Gamma_f + \int_{\Gamma_c} N_i h_c \theta_{\infty} \, d\Gamma_c \quad (14c)$$

The finite element method provides a technique for spatial discretization of the body and construction of shape functions, N_i , for the numerical solution of Eq. (13). Let the domain, Ω , be partitioned into a finite number of four node quadrilateral elements, Ω^e , interconnected at their nodal points, Fig. 2-2.

Having constructed a finite element mesh for the problem, we proceed to construct a corresponding set of shape functions. In constructing the shape functions, we seek a change in coordinates which maps the given quadrilateral into a biunit square (Fig. 2-3). This standardizes the subsequent integration of Eq. (15).

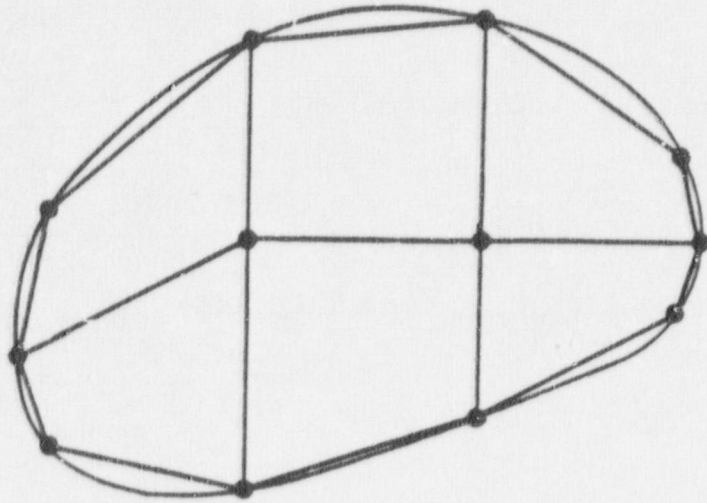


Figure 2-2 Solid body overlaid with a quadrilateral grid.

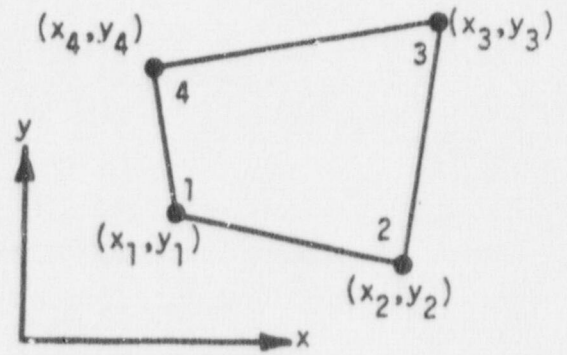
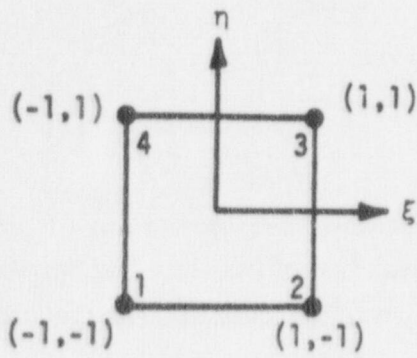


Figure 2-3 Bilinear quadrilateral element domain.

We seek the temperature at the nodal points. This achieves the spatial discretization, and we now require that

$$[C] = \sum_e [C_i^e] = \sum_e \int \int_{\Omega^e} N_i \rho c N_j \, dx dy \quad (15a)$$

$$[H] = \sum_e [H_i^e] = \sum_e \int \int_{\Omega^e} \nabla^T N_i K \nabla N_j \, dx dy + \int_{\Gamma_c^e} N_i h_c N_j d\Gamma_c \quad (15b)$$

$$i=1,2,3,4$$

$$j=1,2,3,4$$

$$e=1,2,\dots,n$$

$$\{F\} = \sum_e \{F_i^e\} = \sum_e \int \int_{\Omega^e} N_i q_g \, dx dy - \int_{\Gamma_f^e} N_i q_f d\Gamma_f + \int_{\Gamma_c^e} N_i h_c \theta_{\Omega} d\Gamma_c \quad (15c)$$

for substitution into Eq. (13).

$$x(\epsilon, \eta) = \sum_{i=1}^4 N_i(\epsilon, \eta) x_i^e \quad (16a)$$

$$y(\epsilon, \eta) = \sum_{i=1}^4 N_i(\epsilon, \eta) y_i^e \quad (16b)$$

where the shape function $N_i(\epsilon, \eta)$ for node i defined as

$$N_i(\epsilon, \eta) = \frac{1}{4} (1 + \epsilon_i \epsilon) (1 + \eta_i \eta) \quad (17)$$

relates points in the biunit square (ϵ, η coordinate system) to coordinates of a point in Ω^e (x, y coordinate system), Fig. 2-3. We also require that the temperature be interpolated by these same shape functions (i.e., the isoparametric concept).

$$\theta(\epsilon, \eta) = \sum_{i=1}^4 N_i(\epsilon, \eta) \theta_i^e. \quad (18)$$

Equation (15) is now written as functions of the new variables ϵ and η . That is, the integrands are expressed in terms of ϵ and η and $dx dy$ is replaced by $d\epsilon d\eta$ times the absolute value of the Jacobian J . In general,

$$\iint_{\Omega} f(x,y) dx dy = \int_{-1}^1 \int_{-1}^1 f[x(\epsilon,\eta), y(\epsilon,\eta)] J d\epsilon d\eta \quad (19a)$$

where

$$J = \begin{bmatrix} \frac{\partial x}{\partial \epsilon} & \frac{\partial x}{\partial \eta} \\ \frac{\partial y}{\partial \epsilon} & \frac{\partial y}{\partial \eta} \end{bmatrix} \quad (19b)$$

Equation (15) is integrated numerically by using a second order Gaussian quadrature in each direction. In general,

$$\int_{-1}^1 \int_{-1}^1 g(\epsilon,\eta) d\epsilon d\eta = \sum_{i=1}^4 g(\epsilon_i, \eta_i) W_i \quad (20)$$

where

i	ϵ_i	η_i	W_i
1	$-1/\sqrt{3}$	$-1/\sqrt{3}$	1
2	$1/\sqrt{3}$	$-1/\sqrt{3}$	1
3	$1/\sqrt{3}$	$1/\sqrt{3}$	1
4	$-1/\sqrt{3}$	$1/\sqrt{3}$	1

Upon integration of Eq. (15) for each element, the element equations are assembled to form the matrix Eq. (13). This equation is solved for the temperature field.

2.3 Time Integration Scheme

The time integration of Eq. (13) is carried out using a generalized trapezoidal method. This method has been shown by Hughes [2] to be unconditionally stable for nonlinear problems. The

method consists of the following family array of algorithms: Find the temperature array, θ_n , n takes the value of $\{0,1,\dots,n\}$, after n fixed-length time steps, Δt , such that

$$F_{n+\alpha} = C_{n+\alpha} \dot{\theta}_{n+\alpha} + H_{n+\alpha} \theta_{n+\alpha}, \quad (21a)$$

$$\dot{\theta}_{n+1} = \dot{\theta}_n + \Delta t \ddot{\theta}_{n+\alpha}, \quad (21b)$$

$$\theta_0 = \theta, \text{ (initial condition)} \quad (21c)$$

where

$$C_{n+\alpha} = C(\theta_{n+\alpha}, t_{n+\alpha}), \quad (21d)$$

$$H_{n+\alpha} = H(\theta_{n+\alpha}, t_{n+\alpha}), \quad (21e)$$

$$\theta_{n+\alpha} = (1-\alpha) \theta_n + \alpha \theta_{n+1}, \quad (21f)$$

$$F_{n+\alpha} = (1-\alpha) F_n + \alpha F_{n+1}, \quad (21g)$$

$$\frac{\partial \theta}{\partial t_{n+\alpha}} = \dot{\theta}_{n+\alpha} = (1-\alpha) \dot{\theta}_n + \alpha \dot{\theta}_{n+1}, \quad (21h)$$

$$t_{n+\alpha} = (n+\alpha) \Delta t. \quad (21i)$$

Equations (21b) and (21f) can be rephrased as

$$\dot{\theta}_{n+\alpha} = \frac{1}{\Delta t} (\theta_{n+1} - \theta_n) \quad (22)$$

and

$$\theta_{n+\alpha} = \theta_n + \alpha(\theta_{n+1} - \theta_n), \quad (23)$$

respectively. Substituting these equations into Eq. (21a) yields

$$\left[\frac{C_{n+\alpha}}{\Delta t} + \alpha H_{n+\alpha} \right] \{\theta_{n+1} - \theta_n\} = \{F_{n+\alpha} - H_{n+\alpha} \theta_n\}. \quad (24)$$

The solution marches forward in time by first solving Eq. (24) for the incremental temperature change vector $\{\theta_{n+1} - \theta_n\}$ and then updating the temperature. In nonlinear problems, C, H, and F may be functions of θ ; thus, iteration must be used to solve Eq. (24) (see Section 3.12).

The parameter α used in transient conduction solutions, is taken to be in the interval $[0,1]$. Some well-known members of this α -family are given below.

α	Solution Method
0	Forward difference; forward Euler
1/2	Midpoint rule; Crank-Nicolson
2/3	Galerkin
1	Backward difference

In the case $\alpha=0$, the method is said to be explicit. For $\alpha < 1/2$, the algorithm is conditionally stable; i.e., stability considerations limit the maximum time step size allowed. For $\alpha \geq 1/2$, the algorithm is unconditionally stable and there are no time step restrictions.

For steady-state analysis, Eq. (13) reduces to

$$[H] \{\theta\} = \{F\} , \quad (25)$$

and the solution is obtained in a single step. For nonlinear problems, iteration is used to solve Eq. (25) (see Section 3.12).

2.4 Thermal Contact Resistance Across an Interface (Slidelines)**

If two parts are placed in contact or across a small gap, there exists a considerable resistance to heat flow from one part to the other. This thermal resistance (known as "contact resistance") is a function of the gap width and gap filler, the physical properties of the contact material, the surface conditions and finish, the contact pressure, and the presence of a fluid or vacuum in the gap between the surfaces. We present an algorithm to couple the finite element heat transfer equations between two parts through a contact resistance across a gap which can be of zero thickness between the contacting surfaces. The surfaces in contact can have dissimilar zoning. For ease of presentation, assume for now that the gap has a finite thickness. It will be shown that the gap thickness factors out of the conductance matrix and is incorporated into a contact resistance term. This allows for a zero thickness gap both in reality (i.e., perfect thermal contact) and for numerical modeling purposes (i.e., the two contacting surfaces coincide in spacial coordinates). Triangles are used to mesh the gap between the contacting surfaces (Fig. 2-4).

** Not validated yet in PC version.

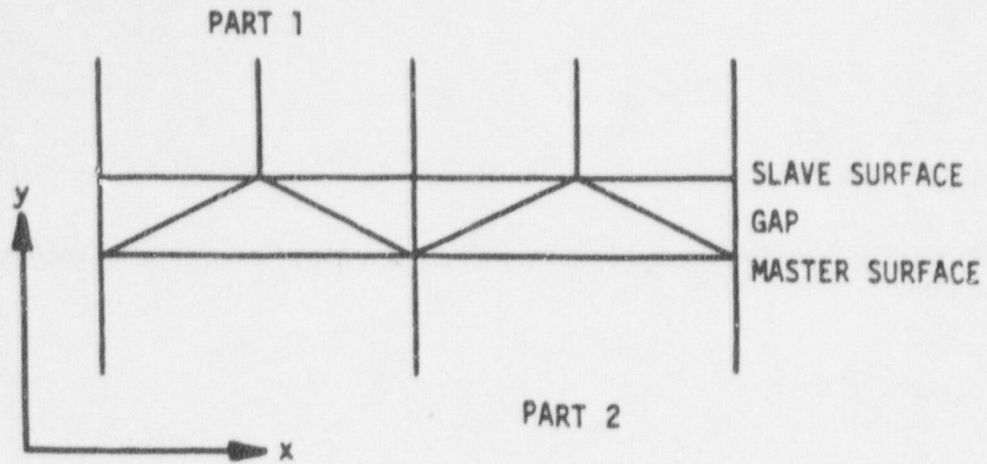


Figure 2-4 Added elements for contact resistance or slideline.

The gap elements are linear triangular elements (4) comprised of an orthotropic material. Consider the triangular element, Fig. 2-5.

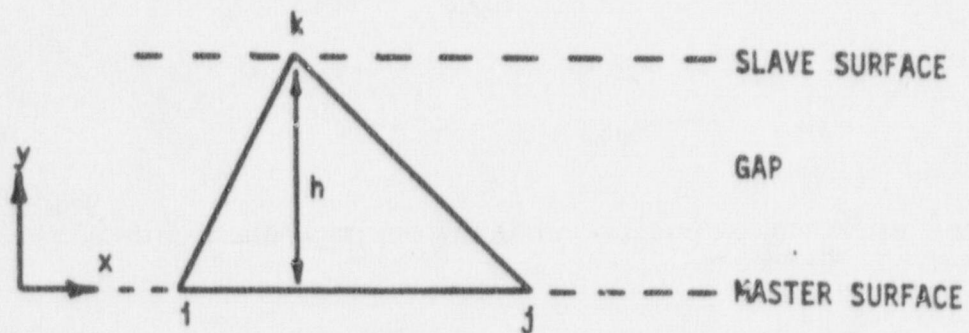


Figure 2-5 Typical triangular element at gap or slideline.

The element conductance matrix is defined as

$$H_{ij} = \int_{\Omega} \nabla^T N_i K \nabla N_j d\Omega , \quad (26)$$

where

$$N_i = (a_i + b_i x + c_i y) / 2A_{ijk} , \quad (27)$$

in which

$$\begin{aligned} a_i &= x_j y_k - x_k y_j \\ b_i &= y_j - y_k \\ c_i &= x_k - x_j \end{aligned} \quad (28)$$

with the other coefficients obtained by a cyclic permutation of subscripts in the order i, j, k . The constitutive matrix is defined as

$$K = \begin{bmatrix} k_x & 0 \\ 0 & k_y \end{bmatrix} \quad (29)$$

Evaluating Eq. (26) using Eqs. (27)-(29) yields the element conductance matrix

$$\begin{aligned} H^e &= \frac{k_x}{4A^e} \begin{bmatrix} b_i b_i & b_i b_j & b_i b_k \\ & b_j b_j & b_j b_k \\ \text{sym.} & & b_k b_k \end{bmatrix} \\ &+ \frac{k_y}{4A^e} \begin{bmatrix} c_i c_i & c_i c_j & c_i c_k \\ & c_j c_j & c_j c_k \\ \text{sym.} & & c_k c_k \end{bmatrix} \end{aligned} \quad (30)$$

Heat transfer is assumed to take place only in the direction perpendicular to the contacting surfaces. Setting $k_x = 0$, Eq. (30) becomes

$$H^e = \frac{k_y}{4A^e} \begin{bmatrix} c_i c_i & c_i c_j & c_i c_k \\ & c_j c_j & c_j c_k \\ \text{sym.} & & c_k c_k \end{bmatrix} \quad (31)$$

The area of the element is

$$A^e = \frac{1}{2} (x_j - x_i) h = \frac{1}{2} c_k h \quad (32)$$

Substituting Eq. (32) into Eq. (31) yields the final result

$$H^e = \frac{1}{2c_k R} \begin{bmatrix} c_i c_i & c_i c_j & c_i c_k \\ & c_j c_j & c_j c_k \\ \text{sym.} & & c_k c_k \end{bmatrix}, \quad (33)$$

where

$$R = \frac{h}{k_y} \quad (34)$$

The term, R , is called the thermal contact resistance. As can be seen from Eqs. (33) and (34), the only place the gap thickness is represented is in the R term. A zero gap thickness is allowable (i.e., perfect thermal contact). However, for computer calculations, R would be assigned a small finite value to prevent a divide-by-zero in Eq. (33). Also, for numerical modeling purposes, the two contacting surfaces can spacially coincide, with the value assigned to R representing the thermal resistance due to a physical gap. For axisymmetric problems, the triangle centroid radius, $r = 1/3 (x_i + x_j + x_k)$, should be included in the numerator of Eq. (33).

If the contacting surfaces are at some angle, ψ , to the global coordinate system, a coordinate rotation must be performed prior to calculating the element conductance matrix, Eq. (33). A local coordinate system is defined with its origin fixed to the global coordinate system and with the x_l axis parallel to the contacting surfaces (Fig. 2-6). Local coordinates are calculated from the global coordinates by

$$\begin{aligned} x_l &= x_g \cos\psi + y_g \sin\psi \\ y_l &= -x_g \sin\psi + y_g \cos\psi \end{aligned} \quad (35)$$

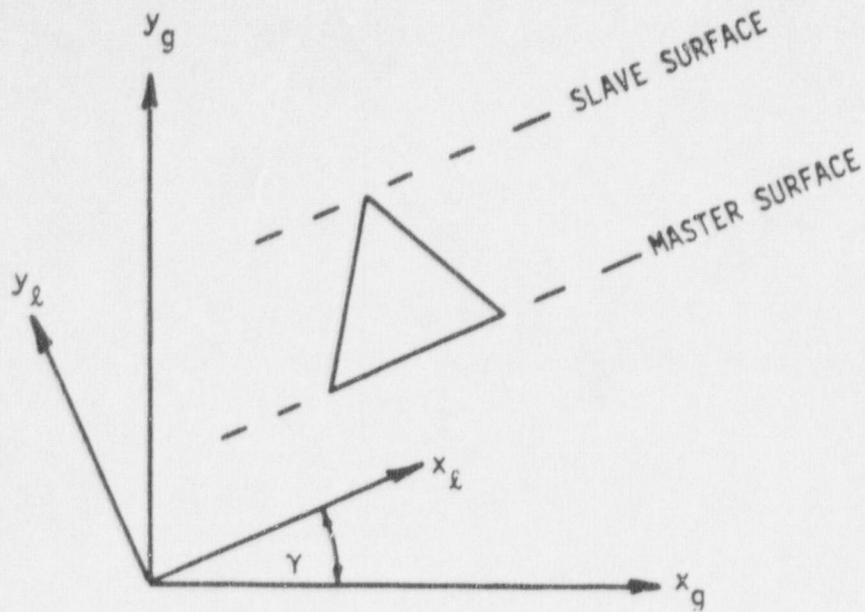


Figure 2-6 Relationship between local and global coordinates.

2.5 Enclosure Radiation**

The finite element thermal analysis of problems involving conduction in a solid coupled with thermal radiation in enclosures (cavities) within the solid can be performed using TOPAZ. The solution procedure is to solve the enclosure radiation problem first for the net radiative flux on each surface, using an estimated initial surface temperature distribution. The resulting fluxes are then used as boundary conditions for the solution of the conduction problem. The conduction solution then gives new estimates for the surface temperatures. The process is then repeated until temperature convergence is achieved.

The enclosure is defined by the discrete boundary surfaces of finite elements which surround the enclosure and define the solid object. Let the finite element of Fig. 2-7 be a boundary element comprising part of the wall of an enclosure. The boundary surface of this element is exchanging energy with other enclosure surfaces by radiation. Additionally, there may be heat transfer from the boundary surface by imposed heat flux or convection. Heat transfer by conduction is occurring within the body. A total energy balance across the boundary surface results in

$$\dot{q}_{\text{COND}} = \dot{q}_{\text{FLUX}} + \dot{q}_{\text{CONV}} + \dot{q}_{\text{RAD}} \quad (36)$$

** Not validated yet in PC version.

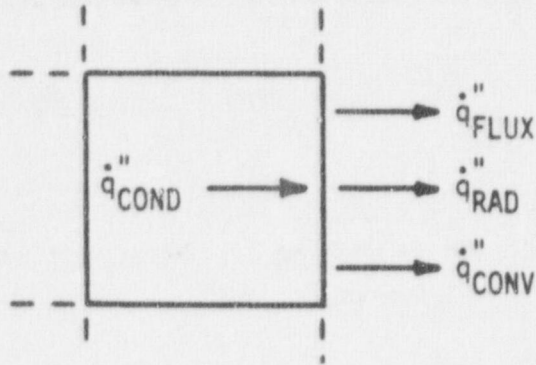


Figure 2-7 Boundary conduction at wall surface.

The radiation term may be calculated separately from any convection or conduction process if the medium within the enclosure does not absorb or emit radiant energy. In the radiation literature this is indicated by specifying

$$\dot{q}_{\text{RAD}}'' = \dot{q}_{\text{NET}}'' \quad (37)$$

Solution Using View Factors

The net radiation heat flux at a surface i is the difference between the emitted radiation and the absorbed portion of the incident radiation.

$$\dot{q}_{i,\text{NET}}'' = \epsilon_i \sigma T_i^4 + \alpha_i H_i \quad (38)$$

Note that Eq. (38) is not a total energy balance at the element surface. Equation (38) is only an expression for the radiation term, \dot{q}_{RAD}'' , for use in Eq. (36).

The radiant flux incident on a surface, H_i (called the irradiation), comes from the other surfaces of the enclosure. Consider the radiation coming from any surface j . An energy quantity called the radiosity,

$$B_j = \epsilon_j \sigma T_j^4 + \rho_j H_j \quad (39)$$

streams away from j in all directions. The first term on the right represents the radiation emitted by the surface, while the second term represents the reflected portion of the irradiation. Of this, an amount $A_j F_{ji} B_j$ arrives at surface i . By employing the reciprocity rule, $A_i F_{ij} = A_j F_{ji}$, this can be rephrased as $A_i F_{ij} B_j$. The rate at which energy arrives per unit area at i from all n surfaces of the enclosure is

$$H_i = \sum_{j=1}^n F_{ij} B_j . \quad (40)$$

The radiosities are found by applying Eq. (39) at each surface of the enclosure. Using the gray body condition $\rho = 1 - \epsilon$ at surface i ,

$$B_i = \epsilon_i \sigma T_i^4 + (1 + \epsilon_i) H_i . \quad (41)$$

Then, using Eq. (40),

$$B_i = \epsilon_i \sigma T_i^4 + (1 - \epsilon_i) \sum_{j=1}^n F_{ij} B_j . \quad (42)$$

In this way there are generated n linear algebraic equations for the n unknown radiosities. The system of Eq. (42) can be rephrased as

$$[\chi] (B) = \{\tau\} , \quad (43a)$$

in which

$$\chi_{ij} = \frac{\delta_{ij} - (1 - \epsilon_i) F_{ij}}{\epsilon_i} , \quad (43b)$$

$$\tau_i = \sigma T_i^4 . \quad (43c)$$

The radiosities are then calculated by

$$(B) = [\chi]^{-1} \{\tau\} . \quad (44)$$

If the surface emissivities are not a function of temperature, then the terms in $[\chi]$ are constant. Thus, the inverse matrix, $[\chi]^{-1}$, need only be calculated once for the problem.

The solution of the enclosure radiation problem proceeds as follows:

1. Compute $[\chi]$.
2. Compute $[\chi]^{-1}$.
3. Guess an initial temperature distribution $\{B\} = [\chi]^{-1} \{T\}_k$.
4. Compute $\{B\} = [\chi]^{-1} \{\tau\}_k$.
5. For $i = 1, 2, \dots, n$ do:

$$\text{Compute } H_i = \frac{1}{1 - \epsilon_i} (B_i - \epsilon_i \sigma T_i^4) ,$$

$$\text{Compute } \ddot{q}_{i, \text{NET}} = \epsilon_i \sigma T_i^4 - \alpha_i H_i .$$

6. Solve the conduction problem for $\{t\}_{k=k+1}$ using $\{\ddot{q}_{\text{NET}}\}$.
7. Repeat steps 4 to 6 until the following criteria are satisfied for prescribed ϵ :

$$\frac{\text{ABS} (\|T_{k+1}\|_2 - \|T_k\|_2)}{\|T_{k+1}\|_2} \leq \bar{\epsilon} .$$

The finite element conduction problem is solved using

$$\ddot{q}_{i, \text{NET}} = \epsilon_i \sigma T_i^4 + \alpha_i H_i , \quad (45)$$

from step 5 as a boundary condition. The T_i^4 term is linearized by using the first two terms of its Taylor series expansion about \hat{T}_i , the temperature from the previous iteration.

$$T_i^4 = 4 \hat{T}_i^3 T_i - 3 \hat{T}_i^4 . \quad (46)$$

Using Eq. (46) in Eq. (45),

$$\ddot{q}_{i, \text{NET}} = 4\epsilon_i \sigma \hat{T}_i^3 T_i - 3\epsilon_i \sigma \hat{T}_i^4 - \alpha_i H_i . \quad (47)$$

The first term on the right contributes to the conductance matrix, while the second and third terms contribute to the load vector.

Solution Using Exchange Factors

TOPAZ can also solve the coupled problem using exchange factors, F_{ij} . The exchange factor is a characterization of the effect of the system geometry, emissivity, and reflectivity on the capability of radiative transport between surfaces A_i and A_j [3].

Using exchange factors, the net radiative heat flux at a surface i is

$$\begin{aligned} \dot{q}_{i, \text{NET}} = & \sum_j F_{ij} (E_i - E_j) \\ & + (\sum_j F_{ij} - F_{ii}) \sigma T_i^4 - \sum_{j \neq i} F_{ij} \sigma T_j^4 \end{aligned} \quad (48)$$

Following the previous procedure, T_i^4 is linearized, and contributions to the conductance matrix and load vector are obtained.

Wavelength-dependent Properties

The gray body assumption becomes prone to error when the range of wavelengths contains strong emission bands, such as for metals. TOPAZ solves problems with wavelength-dependent properties by subdividing the wavelength range into several finite bands and assuming that the surfaces are gray within each band [4]. The net radiative heat flux at a surface i is

$$\dot{q}_{i, \text{NET}} = \int_{\lambda} \dot{q}_{i\lambda, \text{NET}} \, d\lambda \quad (49)$$

with

$$\dot{q}_{i, \text{NET}} = \sigma E_{i, b\lambda} - \alpha_{i\lambda} H_{i\lambda} \quad (50)$$

using view factors or, using exchange factors,

$$\dot{q}_{i\lambda, \text{NET}} = \sum_j F_{ij, \lambda} (E_{i, b\lambda} - E_{j, b\lambda}) \quad (51)$$

The black body band emissive power is calculated by

$$E_{b\lambda} = E_{b\lambda}(\Delta\lambda, T) = f \sigma T^4 \quad (52)$$

The term f represents the fraction of the total radiant output of a black body that is contained in the wavelength band $\Delta\lambda = \lambda_2 - \lambda_1$,

$$f(\Delta\lambda, T) = F_{0-\lambda_2 T} - F_{0-\lambda_1 T}, \quad (53)$$

with [12]

$$F_{0-\lambda T} = \frac{15}{\pi^4} \sum_{m=1, 2, \dots} \frac{e^{-mv}}{m^4} \{[(mv+3)mv+6]mv+6\} \quad v \geq 2, \quad (54)$$

$$F_{0-\lambda T} = 1 - \frac{15}{\pi^4} v^3 \left(\frac{1}{3} - \frac{v}{8} + \frac{v^2}{60} - \frac{v^4}{5040} + \frac{v^6}{272160} - \frac{v^8}{13305600} \right) \quad v < 2, \quad (55)$$

where

$$v = \frac{14388}{\lambda T} \quad (\text{units: } \lambda[\mu\text{m}]: T[\text{K}]). \quad (56)$$

3.0 ASPECTS OF TOPAZ

The sections in this chapter should be consulted prior to and during the construction of TOPAZ input. Many helpful suggestions, warnings, and procedural information are contained in each section.

3.1 Bandwidth Minimization

The Gibbs-Poole-Stockmeyer algorithm [5] coded by S. J. Sackett is available as an option in TOPAZ to minimize the bandwidth and profile of the conductance matrix. The result of bandwidth minimization is a decrease in problem solution time. Bandwidth minimization node-renumbering is transparent to the user. All calculated nodal quantities are printed using the user's original node-numbering scheme.

3.2 Boundary Conditions

As discussed in Section 2.2, heat flux boundary conditions, \ddot{q} , on the boundary are represented by

$$k_x \frac{\partial \theta}{\partial x} n_x + k_y \frac{\partial \theta}{\partial y} n_y = \gamma - \beta (\theta - \theta_\beta) = \ddot{q} \quad (57)$$

Heat flow is positive in the direction of the surface outward normal vector. Surface definition is in accordance with the right-hand rule. The outward normal vector points to the right as one progresses from node N_1 to N_2 (Fig. 3-1).

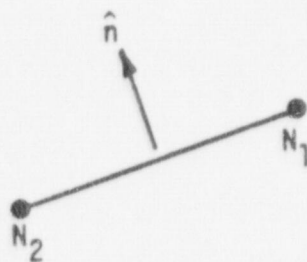


Figure 3-1 Direction of outward normal vector with respect to nodes.

Boundary conditions can be functions of temperature or time. More than one boundary condition can be specified over the same surface, such as in a case of combined convection and radiation. For situations where it is desired to specify adiabatic (i.e., $\ddot{q} = 0$) conditions such as at an insulated surface or on a line of symmetry no boundary condition need be specified. This is the default boundary condition in TOPAZ.

Temperature

Temperature boundary conditions can be specified on any node, whether on the physical boundary or not.

Flux

Set $\ddot{q} = q_f$ where q_f is defined at the node points comprising the flux b.c. segments (Fig. 3-2).

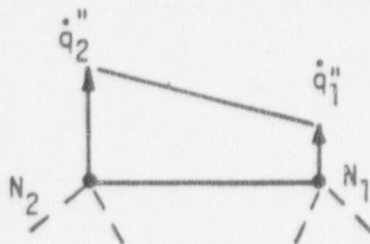


Figure 3-2 Setting boundary linearly varying flux boundary conditions on surface segment.

Radiation

A radiation boundary condition is calculated using a radiant-heat-transfer coefficient. Set $\ddot{q} = h_r (T - T_\infty)$ where h_r is a radiant-heat-transfer coefficient defined as

$$h_r = \sigma F (T + T_\infty) (T^2 + T_\infty^2) \quad (58)$$

The exchange factor, F is a characterization of the effect of the system geometry, emissivity, and reflectivity on the capability of radiative transport between surfaces. The radiation b.c. data cards require specification of the product, $f = \sigma F$, and T_∞ for the boundary segment.

Convection

$$\text{Set } \ddot{q} = h_c (\Gamma - T_\infty)^a (T - T_\infty) \quad (59)$$

where h_c = heat transfer coefficient,
 $(T - T_\infty)^a$ = free convection temperature dependence,
 $(T - T_\infty)$ = temperature potential.

TOPAZ evaluates h_c at the film temperature

$$T_f = \frac{1}{2} (T_{SURF} + T_{\infty}) \quad (60)$$

For forced convection calculations, set $a=0$. Then $\dot{q}'' = hc (T - T_{\infty})$

For free convection calculations, empirical formulas are available to calculate the heat transfer coefficient. These formulas contain the Grashof number raised to some power, a . For example, the average value of the heat transfer coefficient for laminar free convection from an isothermal vertical plate of length L is

$$h_c = \frac{0.555 k_f Pr^{1/4} Gr_L^{1/4}}{L} \quad (61)$$

where the Grashof number is

$$Gr_L = \frac{g \beta_f (T - T_{\infty}) L^3}{\nu_f^2} \quad (62)$$

The rate of heat transfer by convection between the plate and a fluid may be computed by the relation

$$\dot{q}'' = h (T - T_{\infty}) \quad (63)$$

$$= 0.555 \frac{k_f}{L} \left(\frac{Pr g \beta_f L^3}{\nu_f^2} \right)^{1/4} (T - T_{\infty})^{1/4} (T - T_{\infty}) \quad (64)$$

The term

$$= 0.555 \frac{k_f}{L} \left(\frac{Pr g \beta_f L^3}{\nu_f^2} \right)^{1/4} \quad (65)$$

contains constants and material properties which may be a function of temperature. Let h on the convection boundary-condition data-card represent this term. Give the free convection exponent, a , on this data-card a value of 0.25 to account for the term $(T - T_{\infty})^{1/4}$.

3.3 Bulk Fluid**

The bulk fluid concept is best described with the aid of Fig. 3-3:

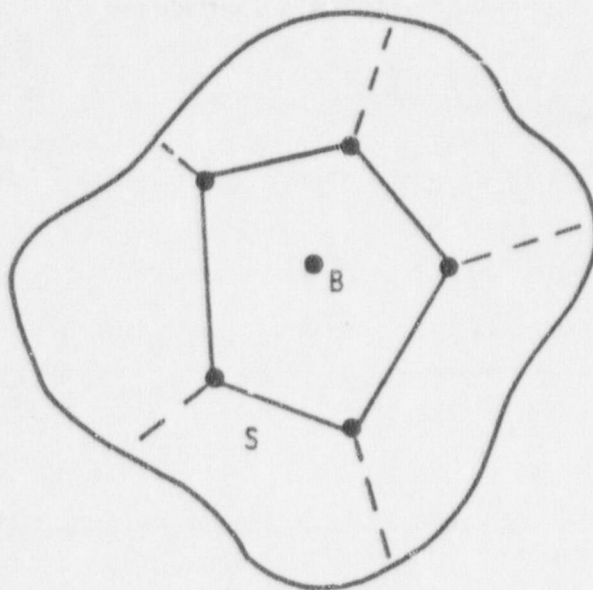


Figure 3-3 Heat flow between bulk node (B) and adjoining surface (S).

Here a bulk node "B" is used to represent the entire volume of a particular material, such as a gas in a cavity. The heat flow between the bulk node (material) "B" and an adjoining surface "S" is given by

$$q'' = f(\theta, t) (\theta_S^a - \theta_B^a)_b, \quad (66)$$

where θ_S and θ_B represent the temperatures of the surface "S" and the bulk node "B," respectively. In addition, the density, specific heat, and volume of the bulk material are specified.

TOPAZ requires that a bulk node be given a node number as well as coordinates. However, these coordinates are arbitrary.

The bulk node concept can also be used in the case where it is desired to specify a lumped heat capacity at a node. In such a case, no segments "S" are associated with the bulk node, and only the density, heat capacity, and volume associated with the bulk node are specified.

** Not validated yet in PC version.

3.4 Element Types

A four node isoparametric element is used. This element degenerates to a three node triangle when the last two node numbers of the four node elements are identical (Fig. 3-4).

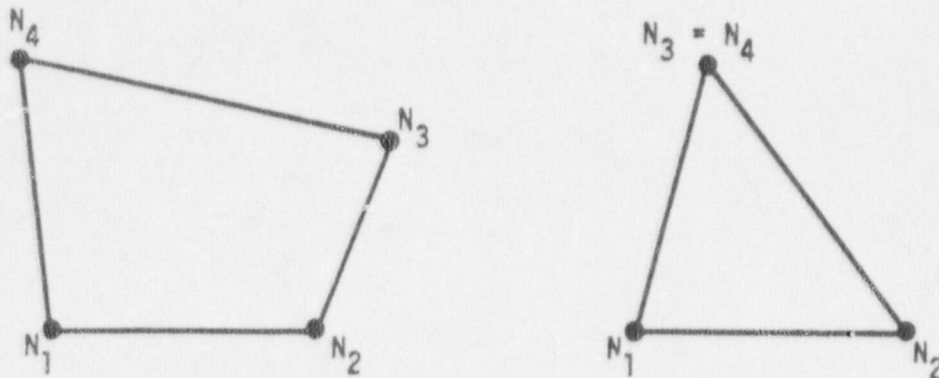


Figure 3-4 Degeneration from four node into three node element.

3.5 Energy Balances**

Various energy terms may be printed and written into the plot file for post processing. The energy terms are:

- change in material internal energy for time step,
- change in material internal energy from initial time,
- heat transfer rates on boundary condition surfaces,
- heat transfer rates on enclosure radiation surfaces, and
- x and y fluxes at all nodes.

Since the nodal fluxes are expensive to calculate, a flag on data section 1 is available to turn this option on or off.

3.6 Function Definitions

Any specified function of time or temperature (for example, internal heat generation, boundary conditions) can be described by either a piece-wise linear curve or by a functional relationship defined in a user subprogram. Functions that are dependent upon both time and temperature must be defined by a User Subprogram.

** Not validated yet in PC version.

A typical piecewise linear curve is shown below in Fig. 3-5.

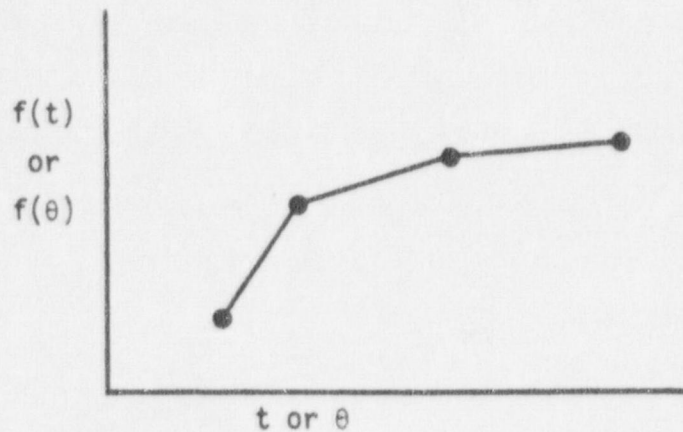


Figure 3-5 Piecewise linear curve for interpolation.

Values of a function at intermediate points on a curve are obtained by linear interpolation. Functional values outside the range of a curve are extrapolated equal to the last value or first value in function curve tables.

A single curve may be used for several functions if their ordinates differ by only a constant. This is accomplished by the use of curve multipliers which are applied to the ordinate of the curve.

In order to differentiate between a function of time and a function of temperature, the sign on the number assigned to the curve describing the function is used. For a time variation, the curve number is positive and for a temperature variation, the curve number is preceded by a negative sign. A curve number of zero indicates that a function is constant.

3.7 Heat Generation

Volumetric heat generation rates may be specified by element, by material, or both (in which case the effect is additive). Volumetric heat generation rates can be functions of time or temperature (see Section 3.6). Spatially, they are assumed constant within an element.

3.8 Initial Conditions

Initial temperature conditions can be specified on the nodal data-input cards or on the nodal temperature initial-condition cards. If no temperatures are specified, the default is 0. For nonlinear steady-state problems, the temperature initial condition serves as a first guess for the equilibrium iterations (see Section 3.12).

3.9 Internal Boundary Elements**

Internal boundary elements allow thermal coupling between two surfaces (e.g., across a gap between two parts) according to the formula

$$q = f(q,t) (\theta_S^a - \theta_B^a)_b. \quad (67)$$

The subscripts A and B refer to the element segments as indicated in Fig. 3-6.

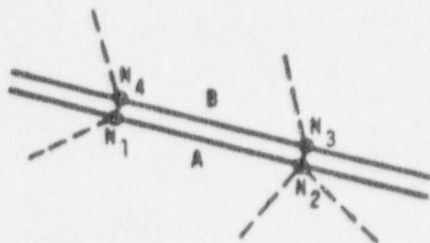


Figure 3-6 Thermal coupling between two surfaces.

θ_A and θ_B are the respective average temperatures of these surfaces. Energy transport is normal to surface A. Segments A and B should be approximately the same length. While four node numbers are required to define this element, opposed nodal coordinates may coincide. That is, an element may have zero thickness. This element is suitable for specifying contact resistances between surfaces and for describing certain types of gaps between surfaces.

3.10 Material Properties

The density, heat capacity, and thermal conductivity are assumed to be spatially constant within each element. Heat capacity and thermal conductivity may be functions of temperature. Since the density and heat capacity appear only as a product in the governing equations, the temperature dependence of the density may be included in the temperature dependence of the heat capacity.

The thermal conductivity may be either isotropic or orthotropic. The orthotropic material angle ψ is defined as shown in Fig. 3-7 below. The orthotropic thermal conductivity matrix, K , is

$$K = \begin{bmatrix} k_{m1} \cos^2 \psi + k_{m2} \sin^2 \psi & (k_{m1} - k_{m2}) \sin \psi \cos \psi \\ (k_{m1} - k_{m2}) \sin \psi \cos \psi & k_{m1} \sin^2 \psi + k_{m2} \cos^2 \psi \end{bmatrix} \quad (68)$$

** Not validated yet in PC version.

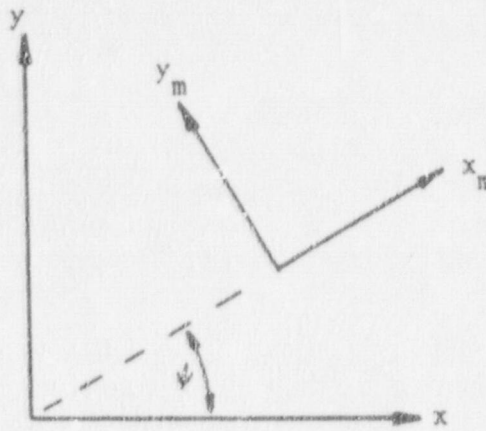


Figure 3-7 Orthotropic material angle ψ .

3.11 Mesh Generation

TOPAZ has no general mesh generation capability. Rows of evenly spaced nodes and rows of sequential elements may be generated internal to the code.

3.12 Nonlinear Analysis

In a nonlinear problem, C , H , and F may be functions of θ , and iteration is required to solve Eq. (24). Functional iteration with under relaxation is used. The nonlinear solution scheme consists of two steps. The first step called "reformation" is the assembly and triangularization of the coefficient matrix

$$\left[\frac{C}{\Delta t} + \alpha K_{n+a} \right] \quad (69)$$

in Eq. (24). This step is computationally expensive. The second step called an "equilibrium iteration" is the formation of the right-hand side vector $(F - K_{n+\alpha}\theta_n)$ in Eq. (24) and back substitution to solve for $(\theta_{n+1} - \theta_n)$. This step is computationally inexpensive.

For strongly nonlinear problems (e.g., radiation boundary conditions), it is necessary to perform a reformation for each equilibrium iteration. For weakly nonlinear problems (e.g., material property nonlinearities), it is computationally advantageous to perform a reformation only at the beginning of the time step, and then to perform as many equilibrium iterations as required for convergence. Further still, a reformation of Eq. (69) can be performed and used over several time steps. It is best to base on experience or a trial-and-error process the decision as to the number of reformations and equilibrium iterations to use on a particular problem.

In a steady-state nonlinear problem, an initial guess should be made of the final temperature distribution and included in the input file as an initial condition. If your guess is good, a considerable savings in computation time is achieved.

3.13 Phase Change

A phase change algorithm developed by Rolph and Bathe [6] has been implemented in TOPAZ. This algorithm explicitly constrains the solution of the conduction problem to satisfy phase change energy balance. Therefore, the finite element mesh and time step size for a specific analysis can be largely chosen by considering the accuracy predicted on the temperatures when phase changes are neglected. The phase change front may advance over several elements in a single time step.

A solution may show temperature oscillations at nodes near the phase change front. This is a result of the algorithm not following the phase change front but, rather, detecting phase change within an element and then lumping material latent heat at the nodes. Spatial discretization and time step size will effect the magnitude and decay rate of these temperature oscillations.

Phase change problems require specification of the problem as a nonlinear analysis with backward difference time integration ($\alpha = 1$) These conditions are automatically invoked on the analysis by setting the phase change calculation flag on control-card one.

3.14 Post Processing

The post processor code PLOTTER in SCANS is available to produce temperature contour plots, flux contour plots, temperature-time history plots, plots of temperature vs distance along arbitrary cut lines, and various geometry plots.

3.15 Radiation in Enclosures**

The theory and algorithms used for enclosure radiation problems are presented in Section 2.5. An enclosure is defined by the discrete surfaces which are, in general, the boundaries of the finite elements which surround the enclosure, as illustrated in the following Fig. 3-8.

13	14	15	16	SEGMENT	NODE	NODE
9	10	11	12	NO.	N1	N2
1	2			1	9	10
16		3		2	10	11
5	4			3	11	7
5	6	7	8	4	7	6
1	2	3	4	5	6	5
				6	5	9

Figure 3-8 Relationship of boundaries for an enclosure.

** Not validated yet in PC version.

The enclosure segments must be specified such that the surface outward normal vector points to the right as one proceeds from node N_1 to N_2 in Fig. 3-8.

When an enclosure has an opening to the exterior of a body, such as surface 6 in Fig. 3-8, the opening acts like a nonreflective surface. Such a surface acts as a blackbody radiator ($\epsilon = 1$) at the outer surrounding temperature. Such surfaces are identified on the enclosure radiation data-cards by flagging them as not participating in the conduction part of the problem and giving them an emissivity curve number of zero.

Emissivity is input as a function of wavelength. If emissivity is considered not a function of wavelength, the first wavelength breakpoint, λ , should be assigned a large number (e.g. 1×10^{10}). Note that the units on the wavelength must be micrometers.

Enclosure radiation problems can be expensive to solve both in computation time and computer core requirements. Problems using view factors that are not a function of wavelength are relatively quick because the $[\chi]$ matrix has to be formed only once for the problem. Problems using wavelength dependent emissivities are computationally slower because a Gauss-Seidel iterative solution is performed to solve the radiation part of the coupled problem for each wavelength band. The radiation part of the coupled problem is performed in-core. For very large problems, an out-of-core solution is available. Contact the author for further information.

3.16 Slidelines - Thermal Contact Resistance Across an Interface**

The theory and algorithm used for slidelines is presented in Section 2.4. Slidelines are used to couple the finite element heat transfer equations between two parts through a thermal contact resistance across a gap between the contacting surfaces. The surfaces in contact can coincide spatially and have dissimilar zoning. One side of the contact surface is referred to as the master surface, and the other side is referred to as the slave surface. The designation of the slave and master surface is arbitrary. However, the slave surface must lie to the left of the master surface, as one moves along the master surface, encountering the master nodes in the order that they are defined (Fig. 3-9).

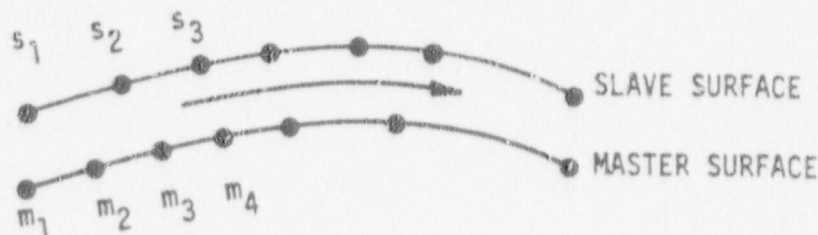


Figure 3-9 Relationship between slave and master surfaces.

** Not validated yet in PC version.

3.17 Steady-State Analysis

TOPAZ has a one step steady-state solution algorithm. For nonlinear steady-state problems, iteration is required, and an initial guess of the temperature field is needed. This can be specified on the initial temperature condition data-cards.

3.18 Thermal Stress Analysis

The temperatures calculated by TOPAZ can be used in performing uncoupled thermal stress analyses with the mechanical code SAPPHIRE (which is included in SCANS). SAPPHIRE will read the temperature states from the plot files generated by TOPAZ.

3.19 Transient Analysis

TOPAZ has both fixed and variable time-step capabilities. In addition, any number of fixed time-step blocks may be specified, allowing for variation of time-step size in a stepwise fashion by restarting the code with new initial temperatures.

3.20 Units

Any consistent set of units may be used with the governing equations.

Examples are:

<u>Quantity</u>		<u>Units</u>	
Temperature	C	C	F*
Space	m	cm	in*
Time	s	s	min*
Density	kg/m ³	g/cm ³	Lb _m /in ³ *
Heat capacity	J/kg C	cal/g C	Btu/Lb _m F*
Thermal conductivity	W/m C	cal/s cm C	Btu/min in F*
Thermal generation	W/m ³	cal/s cm ³	Btu/min ft ³ *
Heat flux	W/m ²	cal/s cm ²	Btu/min ft ² *

* SCANS Units

4.0 EXAMPLES

4.1 Introduction

To validate TOPAZ, six sample problems similar to shipping cask geometry or thermal loadings were run. These sample problems are documented in this manual. Two additional problems benchmark TOPAZ results from SCANS with the mainframe version of TOPAZ.

4.2 Example 1 - Finite Cylinder with Two Surface Temperatures

Carslaw and Jaeger [7] provide a solution for steady-state heat flow in a solid cylinder (Fig. 4-1) with the temperature on the bottom at a fixed temperature and the side and the top at a different temperature. The material thermal properties are held constant (see Fig. 4-1 and Table 4-1). This two-dimensional problem has the exact analytical solution (see Fig. 4-2).

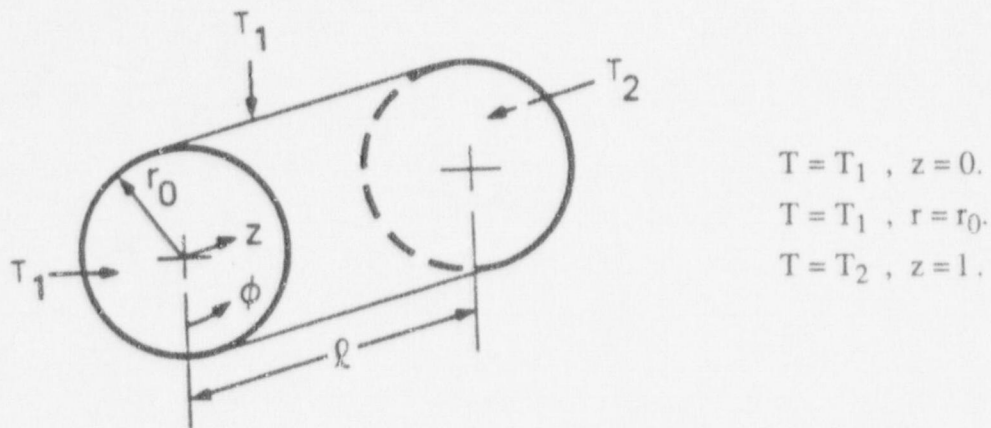


Figure 4-1 Solid finite cylinder with two surface temperatures.

$$\frac{T - T_1}{T_2 - T_1} = 2 \sum_{n=1}^{\infty} \frac{\sinh(\lambda_n Z) J_0(\lambda_n R)}{\lambda_n \sinh(\lambda_n L) J_1(\lambda_n)} \quad (70a)$$

$$J_0(\lambda_n) = 0, \quad Z = z/r_0, \quad L = l/r_0. \quad (70b)$$

Table 4-1 Input data for Example 1.

Geometry

$$l = 10.87313 \text{ m}$$

$$r_o = 2.71828 \text{ m}$$

Boundary Conditions

$$T_2 = 10^\circ\text{C, bottom surface temperature}$$

$$T_1 = 0^\circ\text{C, top/side surface temperature}$$

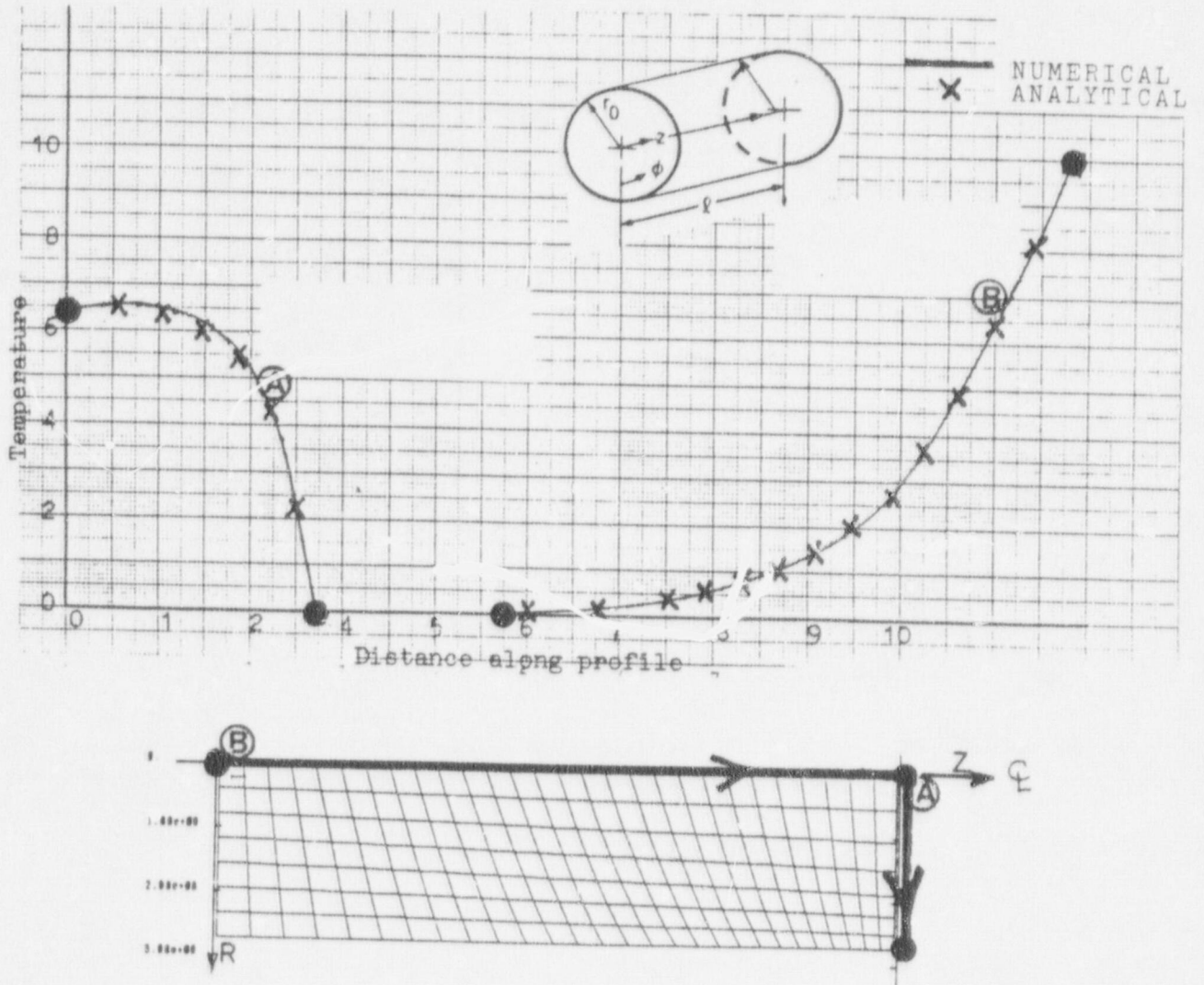


Figure 4-2 Analytical and numerical results for a steady-state heat flow in a finite cylinder with two surface temperatures.

4.3 Example 2 - Slab with Nonlinear Material Properties

Stewart and Wessling [8] analytically solved the following problem, which can be used for comparison in validating heat transfer computer codes. They found that several of the computer codes investigated did not correctly handle strong material nonlinearities.

The problem consists of a homogeneous, isotropic slab of finite thickness, l , heated on the front face by a constant and uniform heat flux, \dot{q} , and insulated on the rear face (see Fig. 4-3 and Table 4-2).

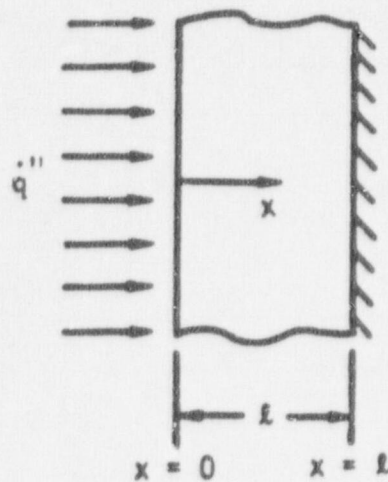


Figure 4-3 Heat conduction in homogeneous isotropic slab.

The appropriate form of the heat conduction equation is

$$\frac{\partial}{\partial x} \left(k \frac{\partial T}{\partial x} \right) + \rho c \frac{\partial T}{\partial t}, \quad (71)$$

subject to the initial and boundary conditions

$$T(x,0) = T_0, \quad (72)$$

$$\frac{\partial T}{\partial x}(0,T) = -\dot{q} / k, \quad (73)$$

$$\frac{\partial T}{\partial x}(l,T) = 0. \quad (74)$$

This problem can be solved analytically for the special case $k = k(T)$, $c = c(T)$, and $\rho = \rho(T)$ such that $k/\rho c = \alpha = \text{constant}$. The solution is

$$\frac{\beta T_0 \theta^2}{2} + \theta = \frac{\dot{q} l}{k_0 T_0} \left(\frac{X^2}{2} - X + \frac{1}{3} + Fo - \frac{2}{\pi^2} \sum_{n=1}^{\infty} \frac{1}{n^2} \cos n\pi X e^{-Fo n^2 \pi^2} \right), \quad (78)$$

where

$$\theta = \frac{T - T_0}{T_0}, \quad (76)$$

$$X = \frac{x}{l}, \quad (77)$$

$$Fo = \frac{\alpha T}{l^2}, \quad (78)$$

Table 4-2 Input data for Example 2.

Geometry and Material Properties

l	=	0.03133 ft
ρ	=	500 lb/ft ³
$k(T)$	=	$k_0 [1 + \beta(T - T_0)] = 1.00 [1 + .005(T - 530)]$ Btu/hr ft °R
$c(T)$	=	$c_0 [1 + \beta(T - T_0)] = 0.005 [1 + .005(T - 530)]$ Btu/lb _m °R
k_0	=	1. Btu/hr ft °R
c_0	=	0.05 Btu/lb °R
β	=	0.005 1/°R

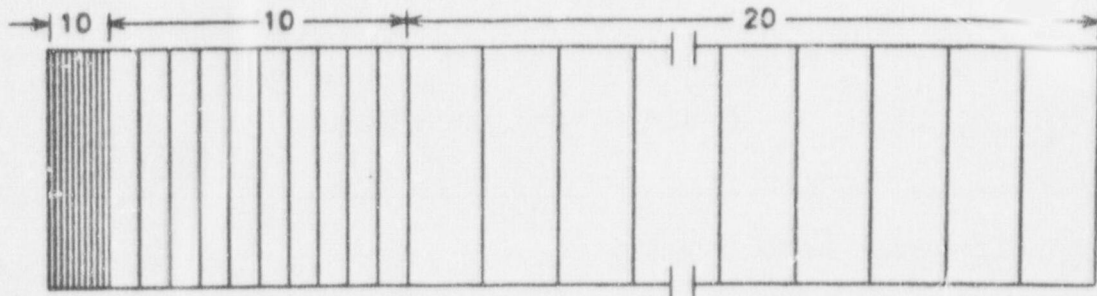
Boundary and Initial Conditions

\dot{q}	=	$2.52 * 10^6$ Btu/hr ft ²
T_0	=	530 °R

The finite element mesh consisted of 40 elements in the x-direction. By trial-and-error, it was found that fewer elements could not resolve the large temperature gradients existing in this program. Table 4-3 shows the analytical and numerical results for the temperature on the face at $x = 0$ at various times.

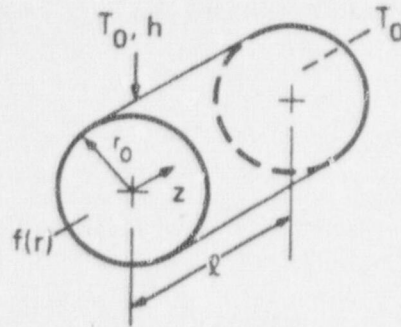
Table 4-3 Comparison of results for Example 2.

TEMPERATURE [$^{\circ}$ R] at $x = 0$		
<u>TIME [hr]</u>	<u>ANALYTICAL</u>	<u>TOPAZ</u>
1×10^{-6}	847.19	845.44
1×10^{-5}	1201.41	1200.24
1×10^{-4}	1851.45	1850.43



4.4 Example 3 - Cylinder with Temperature + Convection Boundary Conditions

Carslaw and Jaeger [9] provide a solution for steady heat flow in a solid cylinder with the temperature on the bottom at a fixed temperature and the side and the top subject to convective cooling. The material thermal properties are held constant. (See Fig. 4-4 and Table 4-4) This two-dimensional problem has the exact analytical solution (see Fig. 4-5):



Finite cylinder with:
 $T = f(r), z = 0, 0 < r < r_0$
 $T = T_0, z = l, 0 < r < r_0$

Convection boundary at
 $r = r_0, 0 < z < l$,
 with h, T_0 .

Figure 4-4 Finite solid cylinder with convection.

$$L = l / r_0, Bi = hr_0/k, \lambda_n J_0'(\lambda_n) + Bi J_0(\lambda_n) = 0, \lambda_n > 0 \quad (79)$$

$$\frac{T - T_0}{T_1 - T_0} = 2Bi \sum_{n=1}^{\infty} \frac{J_0(R\lambda_n) \sin h([1 - z]L\lambda_n)}{(Bi^2 + \lambda_n^2) J_0(\lambda_n) \sin h(L\lambda_n)} \quad (80)$$

Table 4-4 Input data for Example 3.

Geometry and Material Properties

l	=	10.87313 m
r_0	=	2.71828 m
k	=	3 W/m °C, thermal conductivity

Boundary Conditions

h	=	1.10364 W/m ² °C heat transfer coefficient applied over 21
T_0	=	0°C, environment temperature
T_1	=	10°C, environment temperature = $f(r)$

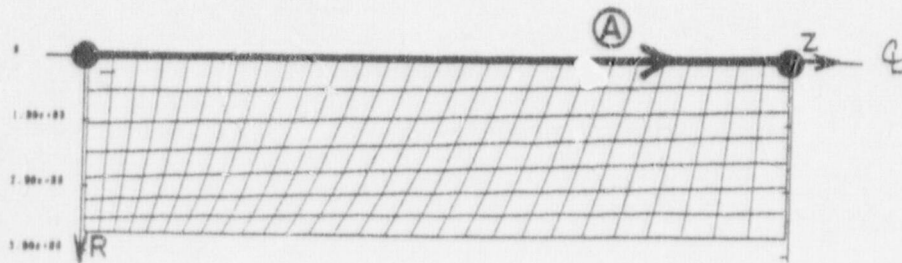
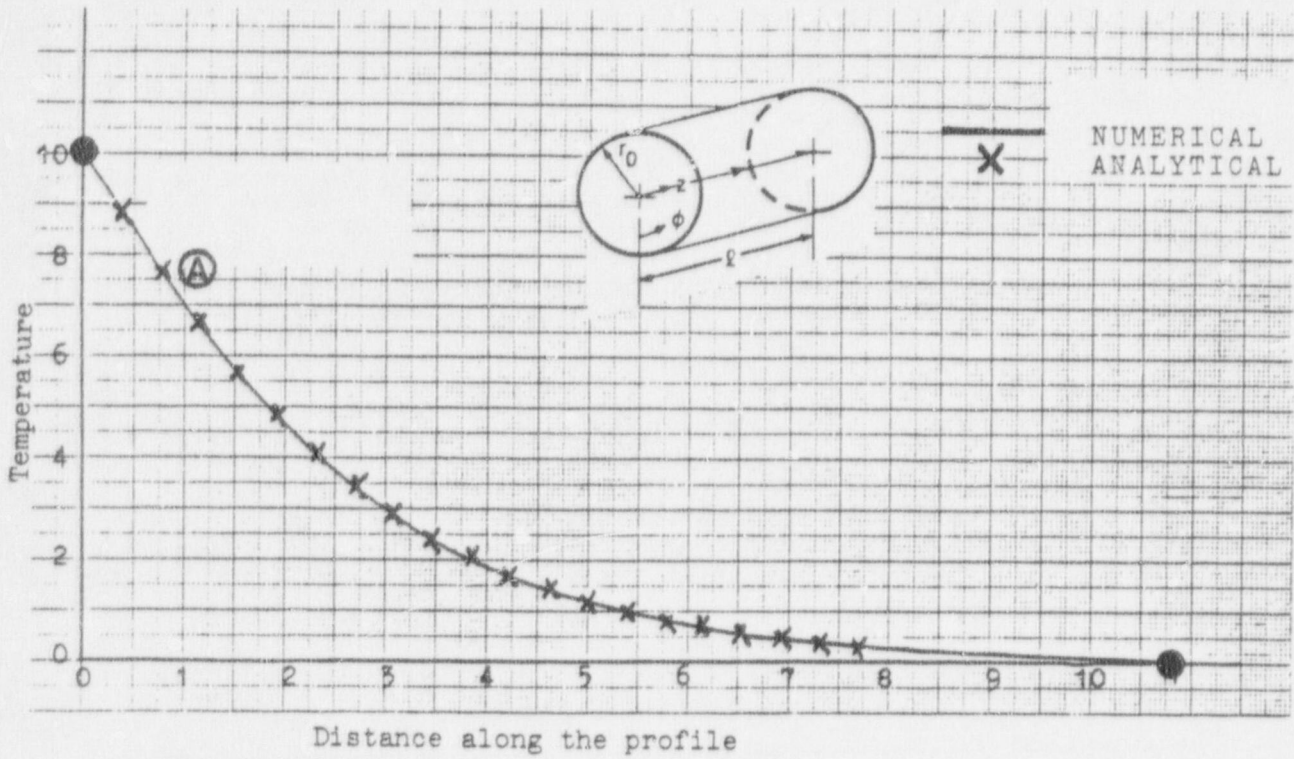


Figure 4-5 Analytical and numerical results of temperature plus convection boundary conditions in a cylinder.

4.5 Example 4 - One-Dimensional Cylinder with Heat-Generating Core

Sandia National Laboratory was contracted to study the performance of general purpose thermal analysis codes used for evaluating the response of nuclear fuel shipping casks to thermal loads. As part of this work, they developed a standard set of thermal models consistent with many shipping cask designs [10]. Model 1 of this standard set consists of a composite two-region cylinder of length L , with a central region that generates heat (Fig. 4-6). The central core (region 1 with $r \leq r_1$) generates heat at 11090 W/m^3 , a value representative of spent fuel shipments, while the external surface of region 2 ($r_1 < r \leq r_2$) is subjected to a convective boundary condition equal to $5.67 \text{ W/m}^2\text{-K}$, simulating natural convection in room temperature air. With all material properties held constant (Table 4-5), this one-dimensional steady-state problem has an exact analytical solution (Fig. 4-7) [10].

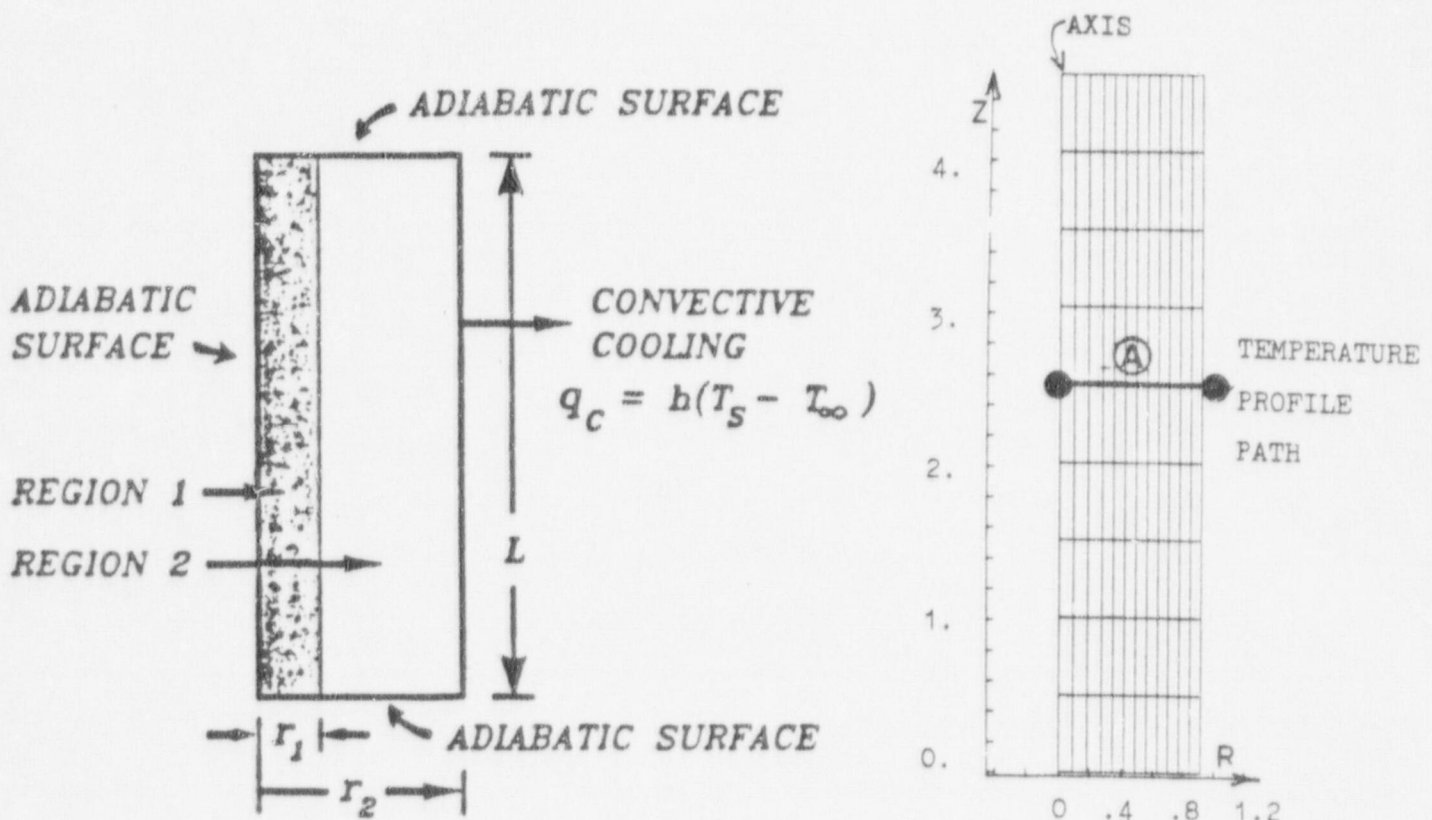


Figure 4-6 SNL Model 1 geometry and LLNL finite element mesh.

The exact solution is:

$$0 \leq r \leq r_1 \quad T(r) = T_\infty + Q r_1^2 \left[\frac{1}{2r_2 h} - \frac{\ln(r_1/r_2)}{2k_2} + \frac{1}{4k_1} \left(1 - \frac{r^2}{r_1^2} \right) \right] \quad (81)$$

$$r_1 \leq r \leq r_2 \quad T(r) = T_\infty + Q r_1^2 \left[\frac{1}{2r_w h} - \frac{\ln(r_1/r_2)}{2k_2} \right] \quad (82)$$

Table 4-5 Input data for Example 4.

Region	Geometry	Material properties*
1	Inner region with internal heat source $r_1 = 0.2743 \text{ m}$ $L = 4.572 \text{ m}$	$\rho_1 = 16.02 \text{ kg/m}^3$ $C_{p1} = 4184 \text{ J/kg-K}$ $k_1 = 69.23 \text{ W/m-K}$ $Q_1 = 11.09 \text{ kW/m}^3$
2	Outer region $r_2 = 0.9144 \text{ m}$ $L = 4.572 \text{ m}$	$\rho_2 = 16.02 \text{ kg/m}^3$ $C_{p2} = 4184 \text{ J/kg-K}$ $k_2 = 34.61 \text{ W/m-K}$

Boundary Conditions

Convective coefficient (h) = 5.67 W/m²-K

Environment temperature (T_∞) = 54.4°C

Initial cask temperature (T_{init}) = 54.4°C

*These material properties not representative of real materials.
The second figure set shows the analytical and numerical results.

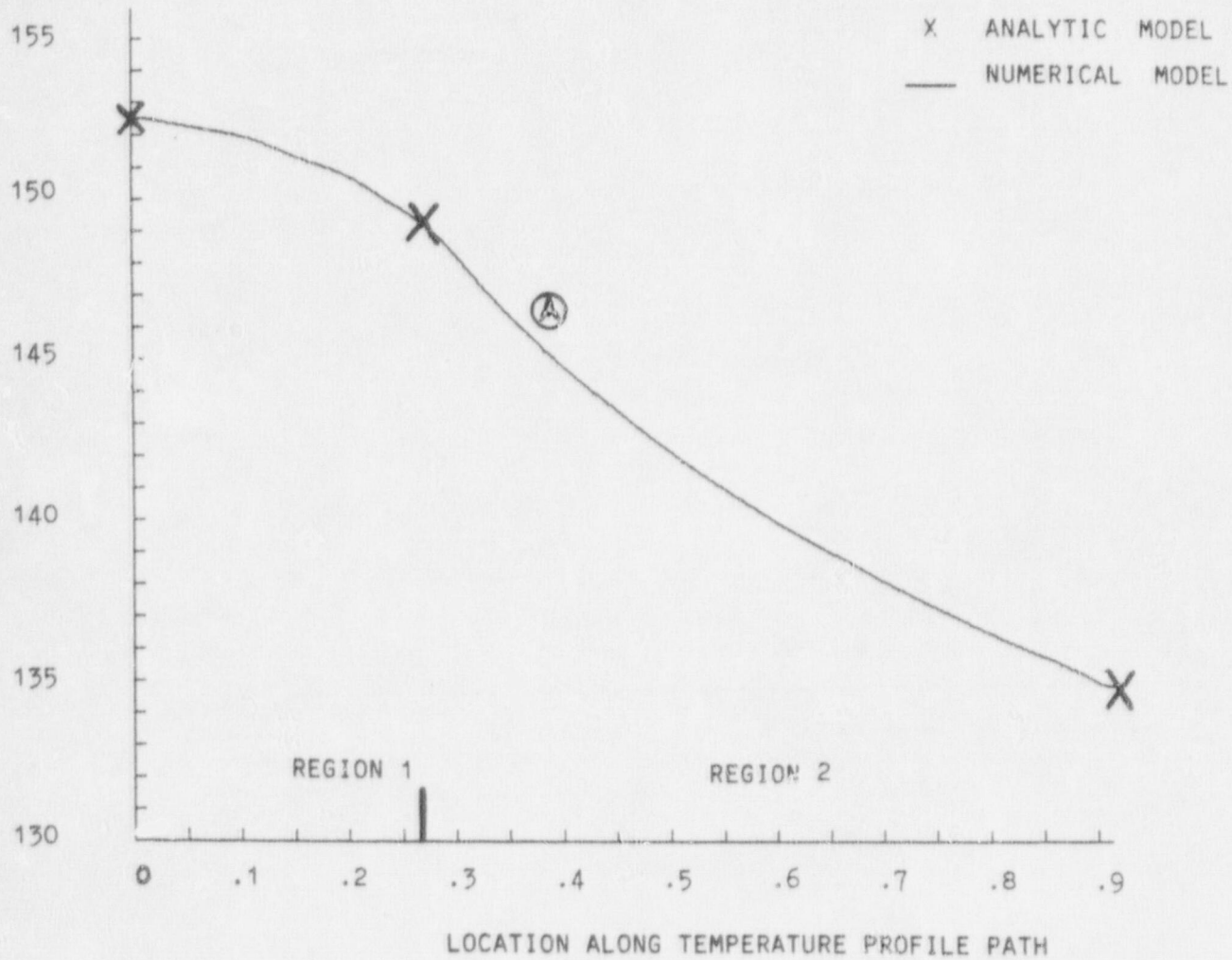
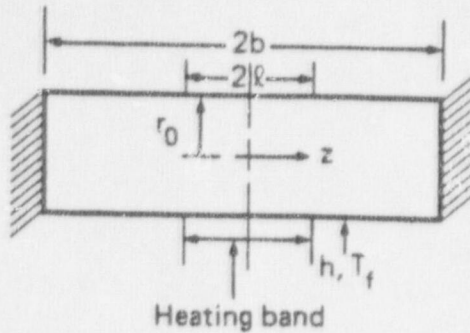


Figure 4-7 Analytical and numerical results for one dimensional cylinder with internal heating.

4.6 Example 5 - Finite Rod with Band Heating

Carslaw and Jaeger [7] provide a solution for steady-state heat flow in a hollow cylinder with a flux boundary condition heat source on the middle of the rod side surface and convection boundary conditions over the entire side surface. The material thermal properties are held constant (see Fig. 4-8 and Table 4-6). This two-dimensional problem has the exact analytical solution (Fig. 4-9):



Finite rod with band heating,
 $q_z = 0, z = \pm b.$
 Convection boundary at $r = r_0,$
 $-b < z < +b.$
 Surface heating (q_s) at $r = r_0,$
 $-l < z < +l.$

Figure 4-8 Finite rod with heating band.

$$\frac{(T - T_f)}{q_s r_0 / k} = \frac{L}{Bi} + 2 \sum_{n=1}^{\infty} \frac{\sin(\lambda_n L) I_0(\lambda_n \rho R) \cos(\lambda_n z)}{\lambda_n [Bi I_0(\lambda_n \rho) + (\lambda_n \rho) I_1(\lambda_n \rho)]} \quad (83)$$

$$\lambda_n = n\pi, Bi = hr_0/k, L = l/b, Z = z/b \quad (84)$$

$$R = r/r_0, \rho = r_0/b \quad (85)$$

Table 4-6 Input data for Example 5.

<u>Geometry and Material Properties</u>	
l	= 5.43657 m
r_0	= 2.71828 m
k	= 3 W/m-K, thermal conductivity
<u>Boundary Conditions</u>	
b	= 2.71828 m
q_s	= 4.41555 W/m ² , heat flux applied over 2b
h	= 1.10364 m, heat transfer coefficient applied over 2l
T_f	= 10°C, environment temperature

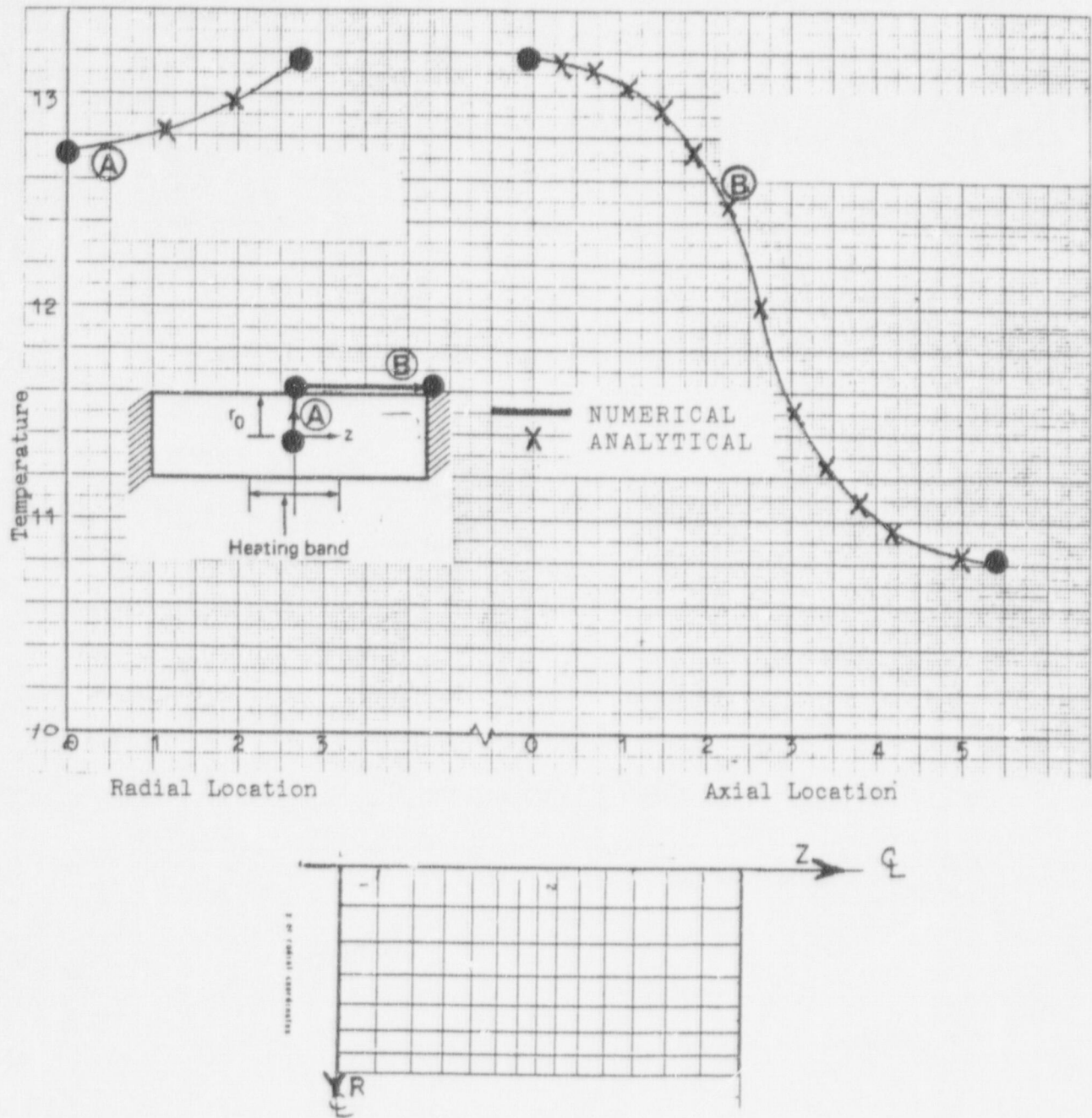
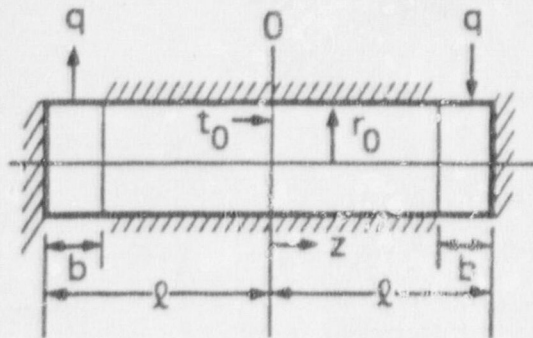


Figure 4-9 Analytical and numerical results for steady-state heat flow in a finite rod with band heating.

4.7 Example 6 - Finite Cylinder with Strip Heating and Cooling

Carslaw and Jaeger [7] provide a solution for steady-state heat flow in a solid cylinder with a heating flux boundary condition source at one end of the cylinder's side surface and an equivalent cooling flux boundary condition at the other end (Fig. 4-10). The material thermal properties are held constant (Table 4-7). This two-dimensional problem has the exact analytical solution (Fig. 4-11):



$$\begin{aligned} q_r &= -q_1, r = r_0, l > x > l - b. \\ q_r &= 0, r = r_0, l - b > z > -l + b. \\ q_r &= +q_1, r = r_0, -l + b > z > -l. \\ q_z &= 0, z = \pm l, r = r_0. \\ T &= T_0, z = 0, 0 < r < r_0. \end{aligned}$$

Figure 4-10 Finite cylinder with strip heating and cooling.

$$\frac{(T - T_0) k}{q_1 l} = \frac{8}{\pi^2} \sum_{n=0}^{\infty} \frac{(-1)^n I_0(m\pi R)}{m^2 I_1(m\pi R_0)} \sin(m\pi b/l) \sin(m\pi Z) \quad (86)$$

where

$$m = 2n + 1, R = r/2l, Z = z/2l, B = b/2l. \quad (87)$$

Table 4-7 Input data for Example 6.

Geometry and Material Properties		
l	=	5.43657 m
r_0	=	2.71828 m
Boundary Conditions		
b	=	1.35914 m
q_s	=	5.5182 W/m ² , heat flux applied over 2b
T_0	=	10°C, center-plane temperature

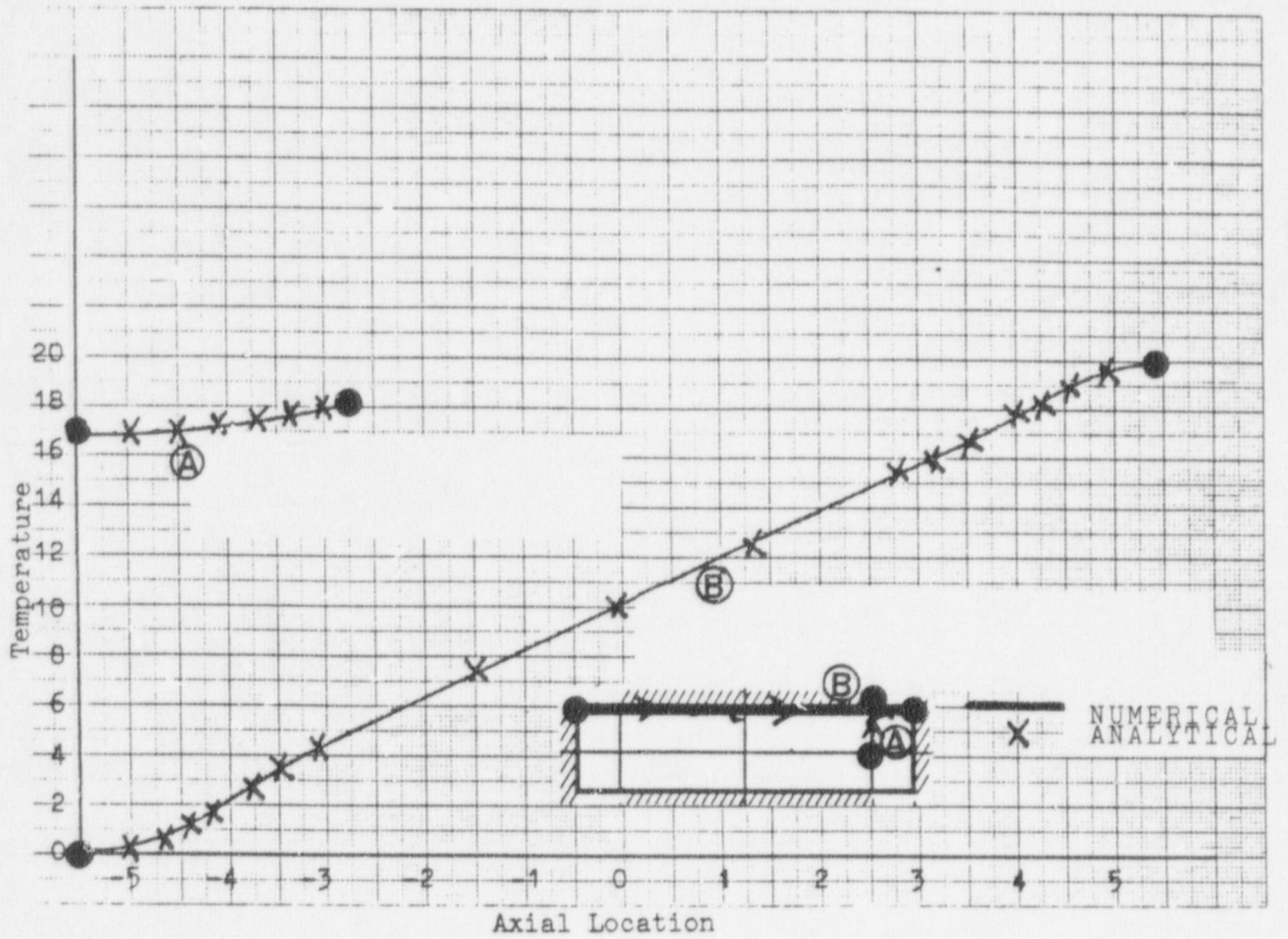
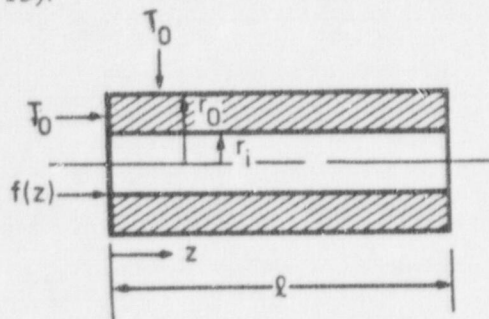


Figure 4-11 Analytical and numerical results for steady-state heat flow in a finite cylinder with strip heating and cooling.

4.8 Example 7 - Finite Hollow Cylinder with Inside Band Heating

Carson and Jaeger [7] provide a solution for steady-state heat flow in a solid cylinder with a flux boundary condition heat source on the middle of the inside surface of the cylinder and fixed temperature boundary conditions over the remaining surface (Fig. 4-12). The material thermal properties are held constant (Table 4-7). This two-dimensional problem has the exact analytical solution (Fig. 4-13):



Finite hollow cylinder with:

$$T = f(z), r = r_1, 0 < z < l.$$

$$T = t_0, r = r_0, 0 < z < l.$$

$$T = t_0, z = 0 \text{ and } l, r_1 < r < r_0.$$

$$\text{For } f(z) = q_1, w < z < (l - w).$$

Figure 4-12 Finite hollow cylinder with inside band heating.

$$F_0 = I_0(n\pi R) K_0(n\pi R_0) - K_0(n\pi R) I_0(n\pi R_0), \quad (88)$$

$$F_1 = I_1(n\pi R_i) K_0(n\pi R_0) - K_1(n\pi R_i) I_0(n\pi R_0), \quad (89)$$

where

$$R = r/l \text{ and } W = w/l. \quad (90)$$

$$\frac{(T - T_0) k}{q_1 l} = \sum_{n=1}^{\infty} \frac{F_0}{n^2 F_1} \cos(n\pi W) \sin(n\pi Z), n = 1, 3, 5, \dots \quad (91)$$

Table 4-8 Input data for Example 7.

Geometry and Material Properties

l	=	10.87313 m
r_o	=	2.71828 m
r_i	=	1 m
k	=	3 W/m-K, thermal conductivity

Boundary Conditions

w	=	2.71828 m
q_1	=	55.182 W/m ² , heat flux applied over w on r_i
T_0	=	0°C, surface temperature

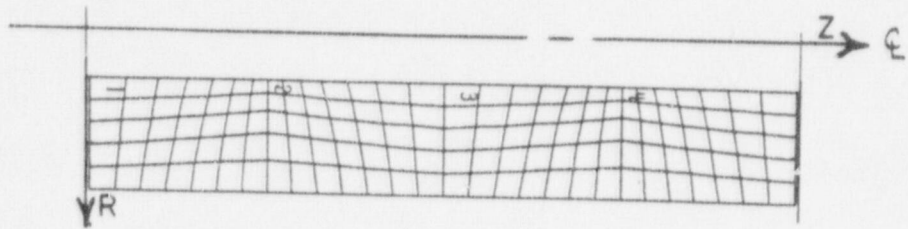
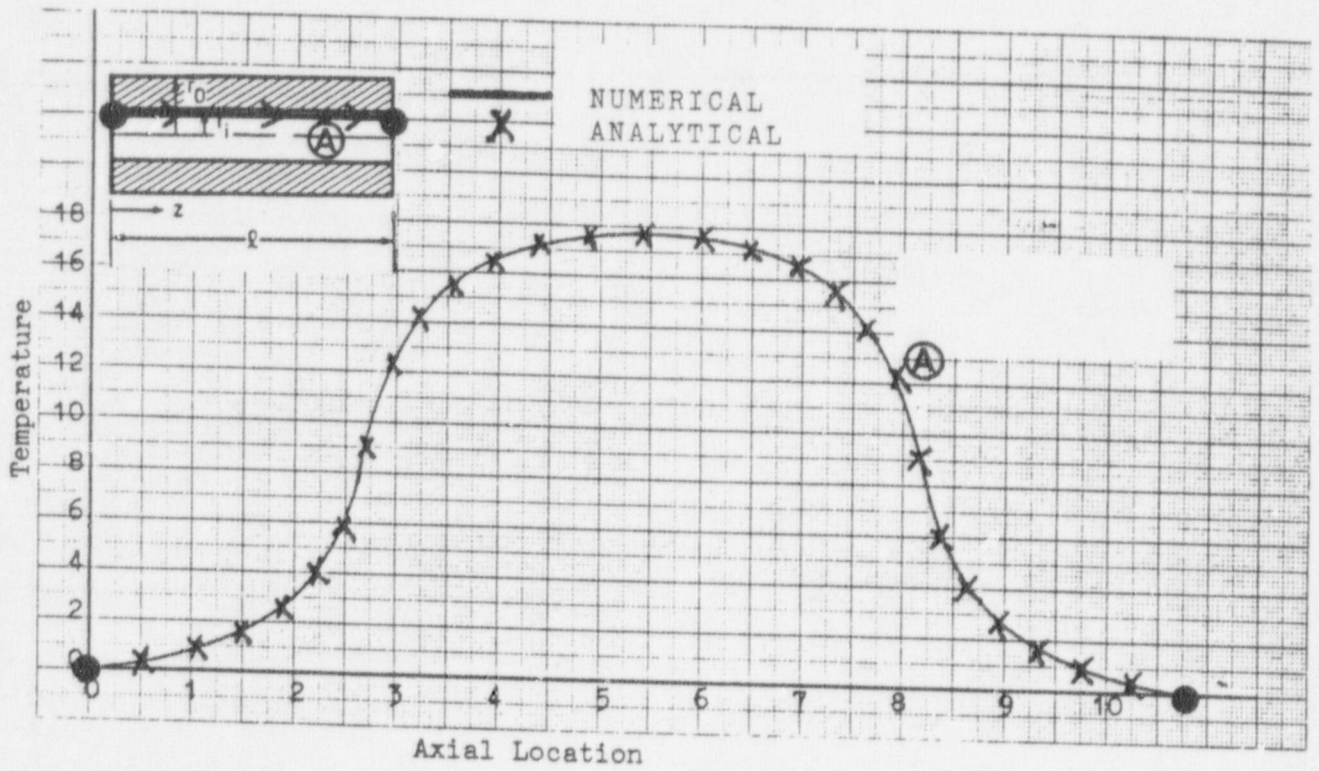


Figure 4-13 Analytical and numerical results for steady-state heat flow in a finite hollow cylinder with inside band heating.

4.9 Example 8 - Regulation Case-Normal Hot Day with Maximum Decay Heat/Solar Heat

Along with Example 9, this case is included to benchmark the PC-based version of TOPAZ with the validated version on the LLNL CRAY mainframe machines. The geometry for this example is similar to some spent fuel shipping cask designs (Fig. 4-14).

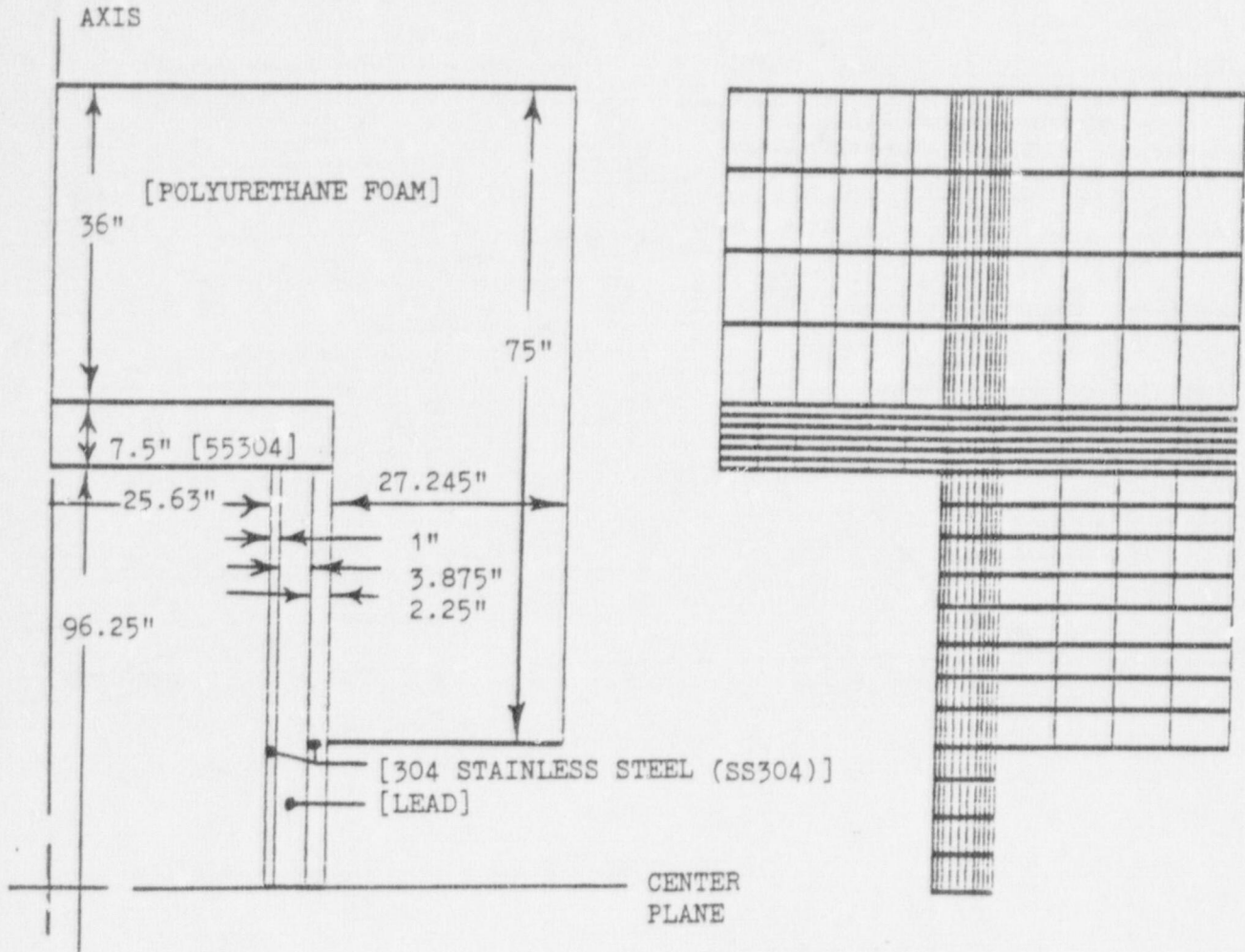


Figure 4-14 Geometry and finite element mesh for regulation case. Normal hot with maximum heat.

The thermal load is based on the regulation-defined case assuming a 100°F ambient temperature with natural convection cooling and 95 Btu/hr-ft² solar heating over the entire external surface. The decay heat, 500 Btu/min, is spread uniformly in terms of an heat flux boundary condition on the surface of the cask cavity. The temperature-dependent heat transfer coefficients for the cylindrical and end surfaces are given by

$$h_{\text{cyl}} = 2.118 \times 10^{-5} (T - T_{\text{amb}})^{1/3} \text{ Btu/min-in}^2 \cdot ^\circ\text{F} \quad (92)$$

$$h_{\text{end}} = 2.095 \times 10^{-5} (T - T_{\text{amb}})^{1/3} \text{ Btu/min-in}^2 \cdot ^\circ\text{F} \quad (93)$$

For stainless steel 304, the density is 0.28414 lbm/in³. The specific heat capacity (Btu/lbm-°F) and the thermal conductivity (Btu/min-in-°F) vs temperature (°F) are given in Table 4-9.

Table 4-9 Stainless steel specific heat capacity and thermal conductivity.

T:	-58.	68.	212.	392.	572.	752.	1112.	1472.
Cp:	.01125	.0114	.012083	.012083	.013056	.013889	.015278	.018056
k:	.12	.123	.12375	.1275	.13125	.135	.1425	.15

For lead, the density is 0.411 lbm/in³. The melt temperature is 620°F, and the heat of fusion is 10.26 Btu/lbm. The specific heat capacity (Btu/lbm-°F) and thermal conductivity (Btu/min-in-°F) vs temperature (°F) are given in Table 4-10.

Table 4-10 Lead specific heat capacity and thermal conductivity.

T:	-58.	68.	212.	392.	572.	630.	717.	1276.
Cp:	.028888	.0280	.0268	.025278	.023889	.016806	.013472	.012028
k:	.03	.0307	.0315	.032598	.033695	.034	.033914	.033653

For polyurethane foam, the density is 0.01157 lbm/in³. The specific heat capacity (Btu/lbm-°F) and thermal conductivity (Btu/min-in-°F) vs temperature (°F) are given in Table 4-11.

Table 4-11 Polyurethane form specific heat capacity and thermal conductivity.

T:	-58.	68.	1300.
Cp:	.000278	.000278	.000278
k:	.3	.3	.3

Figure 4-15 shows a comparison between the CRAY version prediction and the PC version prediction of the temperature profiles along the cask axis and the cask center plane.

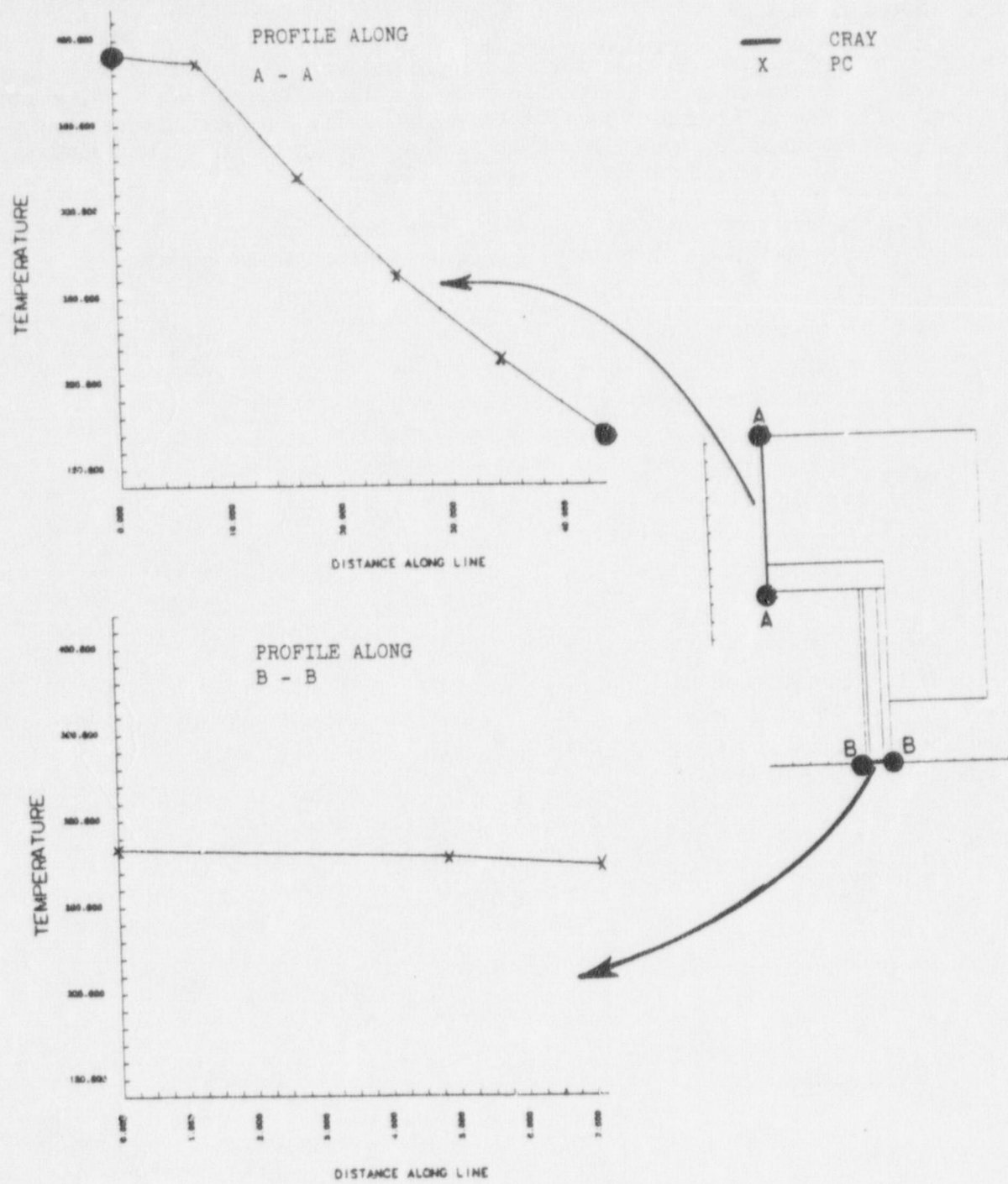


Figure 4-15 Comparison between CRAY version of TOPAZ and the PC version of TOPAZ for Example 8.

4.10 Example 9 - Regulation Case-Cold Soak with Maximum Decay Heat/No Solar Heat

This case is also included to benchmark the PC-based version of TOPAZ with the well-documented version on the LLNL CRAY mainframe machines. The geometry for this example is the same as Example 8. The thermal load is based on the regulation-defined case assuming a -40°F ambient temperature with natural convection cooling over the entire external surface. The remaining input data is the same as Example 8.

Figure 4-16 shows a comparison between the CRAY version prediction and the PC version prediction of the temperature profiles along the cask axis and the cask center plane.

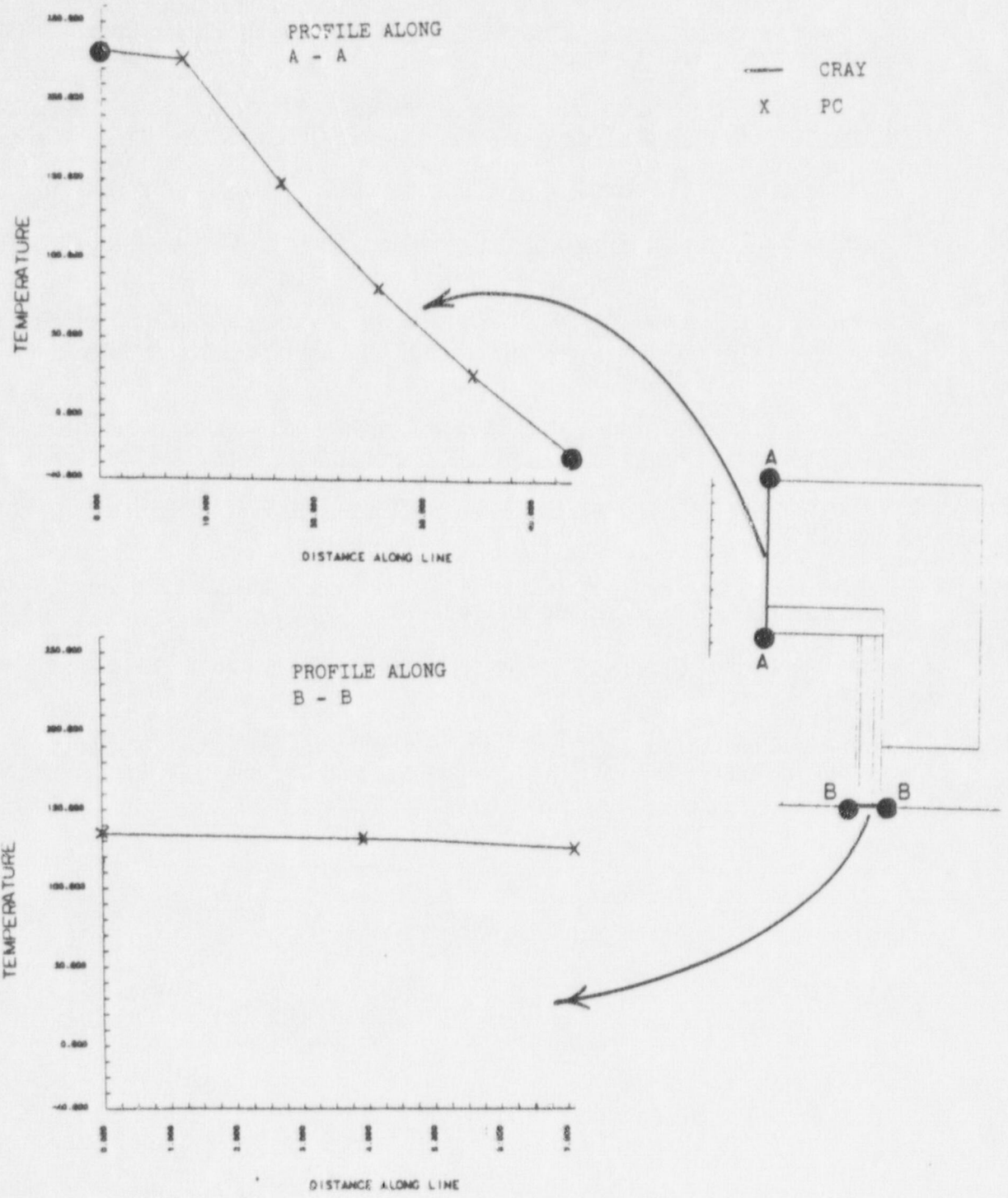


Figure 4-16 Comparison between the CRAY version of TOPAZ and the PC version of TOPAZ for Example 9.

5.0 REFERENCES

1. O. C. Zienkiewicz, The Finite Element Method, McGraw-Hill Book Company (UK) Limited, London, 3rd ed. Appendix 3 (1977).
2. T. J. R. Hughes, "Unconditionally Stable Algorithms for Nonlinear Heat Conduction," Computer Methods in Applied Mechanics and Engineering, Vol. 10, pp 135-139 (1977).
3. H. C. Hottel and A. F. Sarofim, Radiative Transfer, McGraw Hill, New York (1967).
4. R. Siegel and J. R. Howell, Thermal Radiation Heat Transfer, McGraw-Hill, New York (1981).
5. N. E. Gibbs, W. G. Poole, and P. K. Stockmeyer, "An Algorithm for Reducing the Bandwidth and Profile of a Sparse Matrix," SIAM Journal of Numerical Analysis, Vol. 13, No. 2, pp. 236-250 (April 1976).
6. W. D. Ralph III and K. J. Bathe, "An Efficient Algorithm for Analysis of Nonlinear Heat Transfer with Phase Change," Int. J. Num. Meth. Eng., Vol. 18, pp. 119-134 (1982).
7. H. S. Carslaw and J. C. Jaeger, Conduction of Heat in Solids, Oxford University Press, London (1980).
8. R. E. D. Stewart and F. C. Wessling, Jr., "On Heat Conduction in Solids," Sandia National Laboratories, Rept. SC-RR-70-334 (1970).
9. Carslaw and Jaeger, Conduction Heating in Solids, Oxford at the Clarendon Press, Copyright 1959, second edition 1984, pg. 192.
10. L. C. Sanchez, ed., Performance Testing of Thermal Analysis Codes for Nuclear Fuel Casks, Sandia Report SAND84-1854, Sandia National Laboratory, Albuquerque, NM (1987).

BIBLIOGRAPHIC DATA SHEET

SEE INSTRUCTIONS ON THE REVERSE

1. REPORT NUMBER (Assigned by PPMB: DPS, add Vol. No., if any)

NUREG/CR-4554
UCID-20674
Vol. 4

2. TITLE AND SUBTITLE

SCANS (Shipping Cask ANalysis System) A Microcomputer
Based Analysis System for Shipping Cask Design Review
Volume 4: Theory Manual
Thermal Analysis

3. LEAVE BLANK

4. DATE REPORT COMPLETED

MONTH | YEAR
January | 1989

6. DATE REPORT ISSUED

MONTH | YEAR
February | 1989

5. AUTHOR(S)

G.L. Johnson, A.B. Shapiro

7. PERFORMING ORGANIZATION NAME AND MAILING ADDRESS (Include Zip Code)

Lawrence Livermore National Laboratory
7000 East Avenue
Livermore, CA 94550

8. PROJECT/TASK/WORK UNIT NUMBER

9. FIN OR GRANT NUMBER

A-0374

10. SPONSORING ORGANIZATION NAME AND MAILING ADDRESS (Include Zip Code)

Division of Engineering
Office of Nuclear Regulatory Research
U.S. Nuclear Regulatory Commission
Washington, DC 20555

11a. TYPE OF REPORT

Technical

b. PERIOD COVERED (Inclusive dates)

12. SUPPLEMENTARY NOTES

13. ABSTRACT (200 words or less)

TOPAZ is the two-dimensional, implicit, finite-element computer code included in the SCANS cask analysis system for heat conduction calculations. TOPAZ, a code developed on LLNL mainframes, has been implemented on IBM PC computers. This report provides documentation of TOPAZ controls and variables and a description of the numerical algorithms used. Sample problems with analytical solutions are presented.

14. DOCUMENT ANALYSIS - a. KEYWORDS/DESCRIPTORS

analyses of shipping casks
computer code
SCANS

b. IDENTIFIERS/OPEN-ENDED TERMS

15. AVAILABILITY STATEMENT

Unlimited

16. SECURITY CLASSIFICATION

(This page)

Unclassified

(This report)

Unclassified

17. NUMBER OF PAGES

18. PRICE

UNITED STATES
NUCLEAR REGULATORY COMMISSION
WASHINGTON, D.C. 20555

OFFICIAL BUSINESS
PENALTY FOR PRIVATE USE, \$300

SPECIAL FOURTH-CLASS RATE
POSTAGE & FEES PAID
USNRC
PERMIT No. G-67

NUREG/CR-4554, Vol. 4

SCANS (SHIPPING CASK ANALYSIS SYSTEM): A MICROCOMPUTER BASED
ANALYSIS SYSTEM FOR SHIPPING CASK DESIGN REVIEW

FEBRUARY 1989